Climate impacts of the El Niño–Southern Oscillation on South America

Wenju Cai[1,2]✉, Michael J. McPhaden[3], Alice M. Grimm[4], Regina R. Rodrigues[5], Andréa S. Taschetto[6], René D. Garreaud[7,8], Boris Dewitte[9,10,11,12], Germán Poveda[13], Yoo-Geun Ham[14], Agus Santoso[2,6], Benjamin Ng[2], Weston Anderson[15], Guojian Wang[1,2], Tao Geng[1,2], Hyun-Su Jo[2], José A. Marengo[16], Lincoln M. Alves[17], Marisol Osman[18,19], Shujun Li[1,2], Lixin Wu[1], Christina Karamperidou[20], Ken Takahashi[21] and Carolina Vera[18,19]

Abstract | The climate of South America (SA) has long held an intimate connection with El Niño, historically describing anomalously warm sea-surface temperatures off the coastline of Peru. Indeed, throughout SA, precipitation and temperature exhibit a substantial, yet regionally diverse, relationship with the El Niño–Southern Oscillation (ENSO). For example, El Niño is typically accompanied by drought in the Amazon and north-eastern SA, but flooding in the tropical west coast and south-eastern SA, with marked socio-economic effects. In this Review, we synthesize the understanding of ENSO teleconnections to SA. Recent efforts have sought improved understanding of ocean–atmosphere processes that govern the impact, inter-event and decadal variability, and responses to anthropogenic warming. ENSO's impacts have been found to vary markedly, affected not only by ENSO diversity, but also by modes of variability within and outside of the Pacific. However, while the understanding of ENSO–SA relationships has improved, with implications for prediction and projection, uncertainty remains in regards to the robustness of the impacts, inter-basin climate interactions and interplay with greenhouse warming. A coordinated international effort is, therefore, needed to close the observational, theoretical and modelling gaps currently limiting progress, with specific efforts in extending palaeoclimate proxies further back in time, reducing systematic model errors and improving simulations of ENSO diversity and teleconnections.

El Niño and La Niña events denote sea-surface temperature (SST) conditions in the tropical Pacific that are, respectively, warmer and colder than average[1]. Collectively, these events are referred to as the El Niño–Southern Oscillation (ENSO), which, owing to scientific breakthroughs from the 1960s, are now widely known to arise from coupled atmosphere–ocean interactions that, in most cases, involve the entire Pacific basin[2,3]. However, the scientific understanding of ENSO has historically been deeply rooted in South America (SA). For example, El Niño was first described by Peruvian fishermen in the nineteenth century as a warm current appearing around Christmas time along the coast of Ecuador and Peru, disrupting local fisheries and bringing torrential rains to the normally arid coastal plane[4].

Yet, ENSO's effects extend far beyond the coastal regions of Ecuador and Peru, with substantial and regionally varied climatic effects observed throughout the entire SA continent[5–9], as well as globally[1,10,11]. Within SA, changes in temperature and precipitation can be linked to both direct (for instance, coastal warming along Peru[12]) and indirect (for instance, atmospheric teleconnections from the Pacific[13]) forcings, which, in turn, can have marked socio-economic, ecological and environmental impacts. ENSO impacts are felt through agricultural production[14], fisheries[15], malaria occurrence and public health[16,17], wildfire frequency[18], and droughts and floods[19–29]. For example, drought linked to the 1877–78 El Niño led to crop failures, starvation and disease that killed hundreds of thousands in north-eastern Brazil, with similar disruption over the Central Andes[5]. The early 1925 coastal-warming event induced catastrophic floods in the northern region of Peru and Ecuador[12,30], and the ensuing 1925–26 El Niño generated a severe summer drought in the Amazon region, causing deadly fires and the loss of thousands of lives[31]. See BOX 1 for further discussion of ENSO's socio-economic impacts in SA.

✉e-mail: wenju.cai@csiro.au

https://doi.org/10.1038/s43017-020-0040-3

Key points

- The El Niño–Southern Oscillation (ENSO) influences South America (SA) by modifying a unique set of meteorological processes linked to coastal-warming-induced convection, the Walker circulation or Rossby-wave-train-related atmospheric-circulation anomalies.
- El Niño impacts on SA feature a pattern with floods along the west coast of Ecuador and Peru, and Colombia, and drought in the Amazon and north-east of the continent.
- ENSO's impact is modulated by a multitude of factors, including event diversity within ENSO itself, other modes of climate variability within and outside the Pacific, inter-basin climate interactions and greenhouse warming, making its seasonal prediction challenging.
- Greenhouse-warming-induced rainfall reductions can overwhelm El Niño-related rainfall increases, as already found in central Chile, leading to persistent dry conditions.
- Although uncertainty exists, there is a projected intensification of ENSO's impact on SA under greenhouse warming, which is likely to be exacerbated by the mean state change.

The societal relevance of ENSO in SA — a continent of over 420 million inhabitants — provides clear motivation to understand the teleconnections, their mechanisms and their potential change in the future. However, several recent advances in tropical dynamics have also spurred renewed interest in the SA region, building a wealth of literature regarding ENSO–SA teleconnections and necessitating a synthesis of current scientific knowledge. For example, Atlantic SST variability — a product of interactions with the ENSO and ocean–atmosphere processes internal to the tropical Atlantic — has been shown to complicate ENSO's impacts in SA, particularly along the east coast and the interior of the continent[32–34], as occurred in 2012 (REF.[35]). ENSO diversity — for instance, eastern Pacific (EP) or central Pacific (CP) events, which describe where the largest SST anomalies are observed[36,37] — has further been found to have major consequences for understanding corresponding impacts in SA and beyond[38–42], even producing anomalies that are dramatically different from expected in 2015–16 (REFS[43–45]). Interactions with the Indian and Atlantic oceans have also been revealed to feed back to the Pacific, affecting ENSO properties and, thereby, teleconnections[46–49]. Similarly, ENSO's impacts have been shown to be complicated by other modes of natural-climate variability that can interact with ENSO[50–56] and modify its impacts and trends[57]; examples include the Southern Annular Mode[58] (SAM), the Indian Ocean Dipole[50] (IOD), the Interdecadal Pacific Oscillation[59] (IPO), the Atlantic Multidecadal Variability[60] and greenhouse warming[57].

In this Review, we summarize the full scope of ENSO influences on the SA continent, focusing on precipitation given the more direct societal implications through droughts and flooding. We begin by describing the meteorological context of SA, followed by the mechanisms by which ENSO modulates the climate: through local forcing, tropical pathways and extratropical teleconnections. We subsequently outline how ENSO diversity, interaction with other modes of variability and inter-basin interactions govern the corresponding impacts. The Review ends with the implications for predicting and projecting ENSO impacts on SA and identifies the formidable hurdles that must be overcome to enable further progress.

Author addresses

[1]Key Laboratory of Physical Oceanography/Institute for Advanced Ocean Studies, Ocean University of China and Qingdao National Laboratory for Marine Science and Technology, Qingdao, China.
[2]Centre for Southern Hemisphere Oceans Research (CSHOR), CSIRO Oceans and Atmosphere, Hobart, Australia.
[3]NOAA Pacific Marine Environmental Laboratory, Seattle, WA, USA.
[4]Department of Physics, Federal University of Paraná, Curitiba, Brazil.
[5]Department of Oceanography, Federal University of Santa Catarina, Florianópolis, Brazil.
[6]Climate Change Research Centre and Australian Research Council (ARC) Centre of Excellence for Climate Extremes, The University of New South Wales, Sydney, Australia.
[7]Department of Geophysics, Universidad de Chile, Santiago, Chile.
[8]Center for Climate and Resilience Research (CR2), Santiago, Chile.
[9]Centro de Estudios Avanzados en Zonas Áridas (CEAZA), La Serena, Chile.
[10]Departamento de Biología, Facultad de Ciencias del Mar, Universidad Católica del Norte, Coquimbo, Chile.
[11]Millennium Nucleus for Ecology and Sustainable Management of Oceanic Islands (ESMOI), Coquimbo, Chile.
[12]RD/LEGOS, Toulouse, France.
[13]Escuela de Geociencias y Medio Ambiente, Universidad Nacional de Colombia, Medellín, Colombia.
[14]Department of Oceanography, Chonnam National University, Gwangju, South Korea.
[15]Lamont-Doherty Earth Observatory, Columbia University, Palisades, NY, USA.
[16]Centro Nacional de Monitoramento e Alerta de Desastres Naturais, Ministério da Ciência, Tecnologia e Inovação, Sao Paulo, Brazil.
[17]National Institute for Space Research (INPE), São Paulo, Brazil.
[18]Centro de Investigaciones del Mar y la Atmósfera (CIMA/CONICET-UBA), UMI IFAECI/CNRS, Buenos Aires, Argentina.
[19]Facultad de Ciencias Exactas y Naturales, Departamento de Ciencias de la Atmósfera y los Océanos, Universidad de Buenos Aires, Buenos Aires, Argentina.
[20]Department of Atmospheric Sciences, University of Hawai'i at Mānoa, Honolulu, HI, USA.
[21]Servicio Nacional de Meteorología e Hidrologia del Perú (SENAMHI), Lima, Peru.

Meteorological features of the South American climate

We begin by discussing the meteorological features unique to SA, the changes of which determine how ENSO exerts its impact on rainfall and temperature across the continent. From north to south, the South American climate is influenced by the Pacific and Atlantic intertropical convergence zone (ITCZ), the SA monsoon, the South Atlantic convergence zone (SACZ) and the mid-latitude westerly wind belt[61] (FIG. 1a), all of which govern the marked regional variability in seasonal rainfall.

For example, regions north of the equator (such as the Colombian Andes) experience two rainy seasons that peak in April and October (FIG. 1b), related to the twice-yearly meridional movement of the Pacific ITCZ[62–64]. In northern SA, however, most annual rainfall is generated during June-July-August (JJA) (FIG. 1c) when the ITCZ moves north. Further south, rainfall over the Amazon basin (FIG. 1d) is influenced by the SA monsoon[65,66], which starts to develop in late austral spring and peaks in December-January-February (DJF) in the SACZ region (FIG. 1e), when maximum solar radiation reaches the southern tropics.

Monsoonal rain over the Amazon basin during DJF provides moisture to establish an active SACZ[67], the northern edge of which merges with the Atlantic ITCZ. Diabatic heating in the Amazon basin further encourages the establishment of the Bolivian high[68] (FIG. 1a),

Box 1 | **Socio-economic impacts of the El Niño–Southern Oscillation in South America**

El Niño and La Niña are associated with substantial socio-economic impacts in South America, which can often be linked to corresponding changes in precipitation and temperature, thereby, triggering (or amplifying) drought and/or flooding. El Niño-related drought in 1997–98, for example, resulted in a 10% drop in coffee production in Colombia, the country's most important agricultural export[19]. The strong La Niña that followed was further linked to central Chile experiencing the third worst drought in the twentieth century[29], affecting at least 600,000 ha of croplands and fruit plantations, with economic losses of about US$200 million. The compounding impacts of El Niño-related drought and land-use changes increase the vulnerability of ecosystems to fire, with significant consequences for local and regional populations[22]. In Amazonia, for example, the 2015–16 El Niño led to extreme drought conditions, which, in combination with elevated temperatures from global-warming trends[21], increased fire incidence by 36% compared with the preceding 12 years, and pushed active fire detection beyond the agricultural transition zone[18]. Similarly, the 2015–16 El Niño aggravated the effects of a multi-year drought in north-east Brazil that started in 2011–12, with an estimated 33.4 million people affected and economic losses placed at US$26 billion.

Flooding related to the El Niño–Southern Oscillation (ENSO) also has catastrophic impacts. In the Brazilian state of Santa Catarina, flooding during the 1982–83 El Niño event[26] affected 186 of 199 municipalities, leaving 220,000 homeless, 65 dead and/or missing[27] and economic losses exceeding US$1.1 billion[27]. Similarly, in central Chile, three times the average rainfall fell during June-July-August of 1997, resulting in extreme floods that damaged 13,000 houses, caused 21 fatalities and led to economic losses of US$300 million[28]. In addition, in the normally arid coast of Peru, El Niño-related rainfall and flooding[12] in 2017 affected ~1.2 million people and damaged over 50,000 houses and 76,000 ha of croplands[24].

Beyond drought-related and/or flooding-related impacts, ENSO has also been linked to an increase in vector-borne diseases[16,17]. The 1991–92 El Niño, for example, led to a doubling in the number of malaria cases as the regional mean temperature increased and mean rainfall decreased, increasing transmission and favouring the establishment of breeding sites, with similar spikes also observed during the 1997–98, 2006–07 and 2009–10 El Niños. Given these strong socio-economic impacts, there is strong motivation to understanding ENSO teleconnections to South America in both contemporary and future climates to minimize and mitigate potential damage.

which is instrumental in transporting moist air from the interior of the continent to the high-level Altiplano region of the Central Andes. To the south of the Bolivian high, surface heating east of the Central Andes develops a seasonal surface low-pressure system over the Chaco region[69] (the 'Chaco Low', CL, FIG. 1a). The resulting strengthening of the sea-level pressure gradient between the continent (the CL) and the South Atlantic high intensifies the trade winds, encouraging north-easterly or easterly moisture flow from the tropical Atlantic Ocean to the Amazon basin[70]. These interactions produce low-level winds and moisture convergence over the Amazon, central and south-east Brazil, and other tropical/subtropical regions east of the Andes, resulting in the enhanced rainfall in SACZ regions[66,71] during DJF and March-April-May (MAM) (FIG. 1d,e).

After crossing the Amazon basin, the low-level flow is blocked by the Andes and channelled southwards, establishing the South American low-level jet[72] (SALLJ) (FIG. 1a). The SALLJ transports a large amount of moisture from the Amazon to the subtropics, facilitating the development of mesoscale convective systems (MCS in FIG. 1a) in south-east SA (SESA) and contributing to stable, year-round precipitation[72–74] (FIG. 1f). The SALLJ can manifest in two regimes: strong southwards flow that transports moisture from the Amazon basin to the SESA region (which is more prevalent in JJA) and a weak eastwards flow that redirects moisture to the SACZ (which develops more often in DJF, increasing rainfall in south-east Brazil)[71,73]. After March, the SA monsoon weakens as the area of deep convection retreats north-westwards and drier conditions return to the subtropical SA, leading to a declining moisture supply to the SACZ. In north-east Brazil, the rainy season takes place during March through May (FIG. 1g), when the Atlantic ITCZ is in its southernmost position.

As the seasons advance, the SACZ weakens and disappears by JJA, while the Atlantic ITCZ moves northwards (FIG. 1a) and the Amazon enters its dry season (FIG. 1d). With cooler temperatures, the CL and the Bolivian high vanish. However, the Atlantic subtropical high strengthens and expands westwards, such that the pressure gradient between the continent and the Atlantic subtropical high strengthens, in turn enhancing the SALLJ[72]. Likewise, the Pacific subtropical high is furthest to the north and closest to the continent in JJA, so central Chile (30°S – 40°S) and the adjacent Andes, therefore, experience their rainy season during this time, given links to frontal systems moving from the Pacific, cut-off lows[75] and atmospheric rivers[76] (FIG. 1h). By contrast, to the south of 45°S, the westerly wind belt is present year-round, resulting in a weak annual cycle of rainfall, with large accumulations (>3,000 mm year^{-1}) over the western side of the austral Andes and dry conditions to the east of the continental divide[77].

Mechanism for ENSO impact

As a result of random fluctuations in the climate system and coherent modes of climate variability, the most significant of which is ENSO, rainfall and temperatures can deviate from the average conditions described previously. This section describes the main mechanisms by which ENSO impacts the South American climate: direct local forcing in the coastal zone of western SA and remote forcing via two far-field atmospheric-teleconnection pathways through the tropics and extratropics. Emphasis is placed on understanding the dynamics and impacts associated with a typical El Niño event, as reflected by the standardized regressions shown in FIG. 2, which assumes that El Niño and La Niña events are symmetrical but opposite in sign.

Local forcing

During an El Niño event, anomalously warm waters are often observed adjacent to western tropical SA, particularly in a coastal El Niño[12,78], with a typical magnitude of 1.5–3 °C. Through transferring heat from the ocean to the atmosphere, this anomalous warming elevates air temperatures in the coastal region, triggering localized atmospheric convection and heavy rainfall. The rainfall impacts on the coast of Ecuador and Peru occur mainly in the rainy months of February, March and April, when regional SSTs are seasonally at their highest and the threshold for deep convection is more likely to be reached. However, coastal warming off the coast of Peru and Ecuador also causes a decrease in the SST gradient with the far-eastern Colombian Pacific, weakening transport of moisture to the region and, thereby, contributing to drought over Colombia[62,64]. Warm and cold events exhibit marked asymmetry with their impacts, related to the ability of anomalies to push the SST above convection thresholds[79].

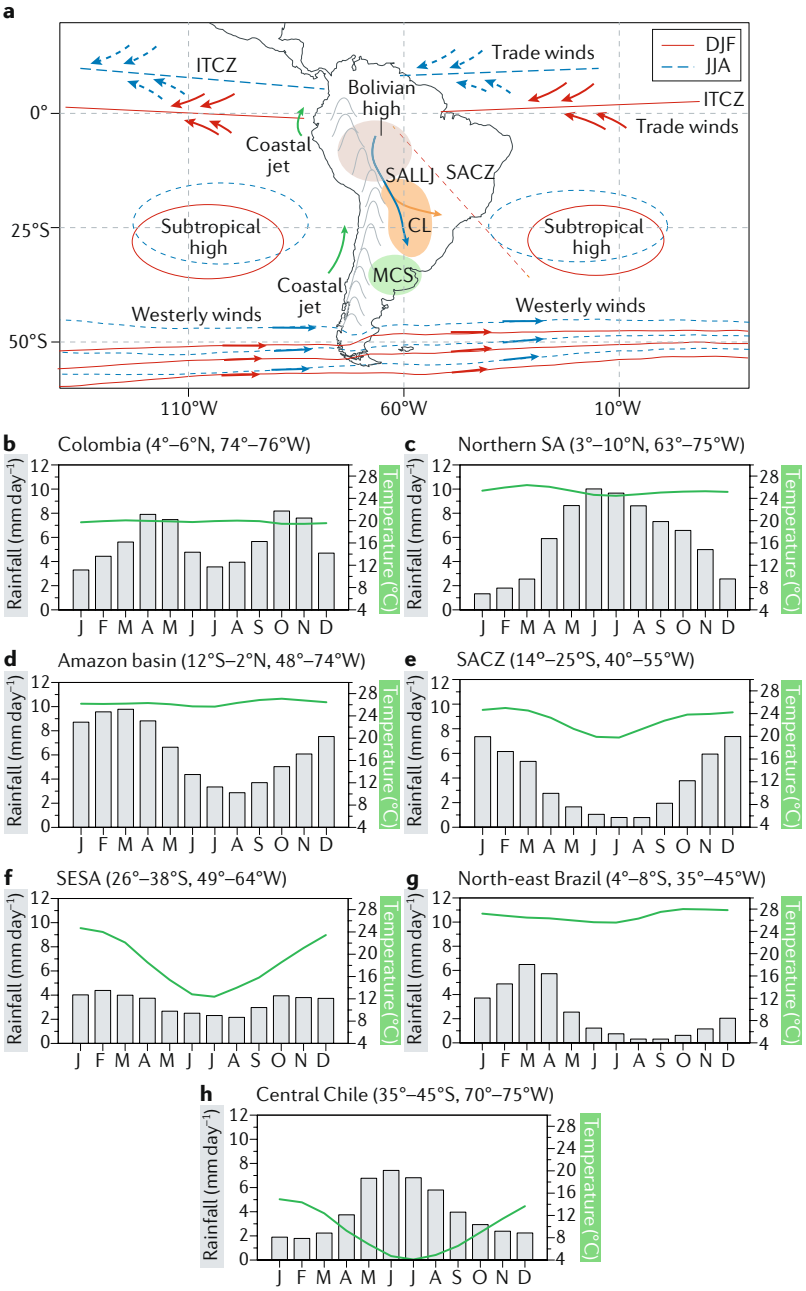

Fig. 1 | **South American meteorological and climatological features.** Schematic of the main climatological features in South America (SA) (part **a**). The blue and red lines represent features in June-July-August (JJA) and December-January-February (DJF), respectively. Seasonal climatology of rainfall[190] (bars) and air temperature[191] (lines) for seven regions: Colombian Andes (part **b**), northern SA (part **c**), Amazon basin (part **d**), south-east Brazil over the SACZ region (part **e**), south-east SA (SESA) (part **f**), north-east Brazil (part **g**) and central Chile (part **h**). The South American climate, therefore, features a set of unique processes that govern the strong regionality of the seasonal cycle, which the El Niño–Southern Oscillation modifies to exert its impact. CL, Chaco Low; ITCZ, intertropical convergence zone; MCS, mesoscale convective system; SACZ, South Atlantic convergence zone; SALLJ, South American low-level jet.

Tropical pathway

Anomalous ENSO-related SSTs also drive changes in the climatological Walker circulation (FIG. 2a), which refers to a series of zonal overturning cells in the atmosphere associated with regions of rising and sinking motion. This so-called tropical pathway refers to the eastwards shift in deep convection that occurs as a result of anomalous SST warming in the central and eastern equatorial Pacific (FIG. 2b), pushing average SSTs above the thresholds for atmospheric convection. These changes in the Walker circulation further promote anomalous descending motion over much of eastern equatorial SA and the western equatorial Atlantic during September-October-November (SON) and DJF, where the coldest surface temperatures are located[80–83] (FIG. 2c,d), inhibiting the equatorwards movement of the Atlantic ITCZ and contributing to negative precipitation anomalies over equatorial eastern SA. By MAM, subsidence shifts to the eastern equatorial Atlantic. However, dryness over the equatorial eastern SA is enhanced by the tropical Atlantic meridional SST gradient (FIG. 2e), driven by extratropical teleconnections.

Extratropical pathway

In addition to being affected by the anomalous Walker circulation, ENSO impacts in SA are also modulated by an extratropical teleconnection. This extratropical pathway refers to a pattern of stationary Rossby wave trains — triggered by anomalous convection over the tropical Pacific — and describing a series of positive and negative atmospheric-pressure anomalies that extend northwards and southwards into the mid-latitudes, before then veering into the Atlantic basin[80–82,84,85] (FIG. 2c,d). In the northern hemisphere, these wave trains are referred to as the Pacific–North American (PNA) pattern[86,87], and in the southern hemisphere, the Pacific–South American (PSA) pattern[88–90].

Owing to the strength of ENSO anomalies[91] and the equator-to-pole temperature gradient[80], the PSA is most pronounced during SON. During an El Niño event, the atmospheric pattern culminates in negative and positive pressure anomalies over the eastern mid-latitudes and eastern subtropical SA, respectively (FIG. 2c). These atmospheric-circulation anomalies favour north-westerly advection of moist warm air into SESA, as well as an enhanced SALLJ[76,92,93]. Collectively, such features, combined with favourable synoptic meteorological

conditions, promote heavy rainfall and flooding across southern Brazil, Uruguay and northern Argentina[26,82,94] (FIG. 2c). The PSA further induces positive pressure anomalies over the Amundsen and Bellingshausen Seas, blocking the westerly winds, displacing the storm track to the north and favouring more frequent passage of frontal systems over central Chile and the subtropical Andes, especially during JJA, the major rainy season[95].

The PNA, by contrast, attains maximum amplitude during DJF and is able to influence the climate of northern SA through the presence of anomalous cyclonic circulation over the western tropical North Atlantic (FIG. 2d). The cyclonic anomalies, in combination with a corresponding weakening of the trade winds[96] and wind-evaporation-SST feedbacks[97,98], promote warmer SSTs in the tropical North Atlantic from February through May[99,100], referred to as the Atlantic Meridional Mode. This warming pattern inhibits the southwards migration of the rain-bearing Atlantic ITCZ, resulting in negative rainfall anomalies in north-east Brazil[40,99,101] and the Amazon basin[42,80,99] (FIG. 2e). Conversely, La Niña events tend to generate cold SST anomalies in the tropical North Atlantic region, reinforcing the southwards shift of the ITCZ and bringing anomalously high rainfall to northern SA. Together with the PSA-related positive rainfall anomalies in the south, the PNA-related negative rainfall anomalies in the north contribute to a well-known, large-scale dipole structure that characterizes SA rainfall variability associated with an El Niño event (FIG. 2c–e).

Impact on air temperatures

In comparison to rainfall, ENSO signatures in surface-air temperatures are relatively modest[9,102]. Temperature impacts vary seasonally and are governed by a variety of processes operating in tropical and extratropical regions[102,103]. During an El Niño, for example, cooler surface-air temperatures in SESA tend to coincide with rainier conditions due to cloud radiative impacts on insolation. However, more rainfall often accompanies enhanced northerly flow of warm air and, as such, the balance between warm advection and cold conditions associated with rainfall acts to produce relatively low-amplitude air-temperature anomalies. These effects are particularly noticeable over the southern half of the continent (FIG. 2c–e). A notable exception occurs during JJA of El Niño years when the northerly flow is intensified with no corresponding rainfall anomalies, favouring unusually warm conditions over the subtropical region east of the Andes[9] (FIG. 2b). Along the tropical west coast of SA, pronounced temperature anomalies also occur at the height of El Niño and La Niña events (FIG. 2d,e).

Diversity of the ENSO and impact on SA

The previous section described the general mechanisms and impacts of ENSO on the South American climate. However, as no two ENSO events are exactly alike (for example, exhibiting different spatial patterns, amplitude and temporal evolution), and as El Niño and La Niña are not mirror images of each other, the climatic impacts may exhibit substantial asymmetry. In this section, we outline the causes and implications of ENSO asymmetry and diversity on subsequent SA climatic impacts.

CP and EP ENSO

ENSO SST anomalies exhibit a longitudinal continuum in the location of maximum amplitude, incorporating EP and CP El Niño and La Niña events[45,79,104,105], which have the largest anomalies in the EP and CP, respectively[36,106] (FIG. 3a, inset). In general, EP El Niños tend to attain stronger SST anomalies than CP El Niños, whereas CP La Niñas tend to be stronger than EP La Niñas[104]. The mechanisms responsible for this diversity in ENSO-related SST location and magnitude involve a diverse mix of oceanic and atmospheric processes, including equatorial upwelling (which tends to be most active in the EP)[45,104], wind-driven zonal displacements of the western Pacific warm pool (which are more influential in changing SSTs in the CP)[107,108] and non-linear atmospheric convection responses to SST (which explain the greater magnitude of El Niño events over La Niña events)[79,106,109].

Given these contrasts, different indices are needed to characterize the diversity of ENSO events, as well as the asymmetry between El Niño and La Niña[104,105]. Many indices have been developed to capture this range of behaviour[104]. Here, we characterize the asymmetry using a linear combination of the first two empirical orthogonal functions of SST anomalies in the tropical Pacific, which capture the essence of EP and CP El Niños in a compact mathematical formulism[37]. The principal components (PCs) of these empirical orthogonal functions, which exhibit a non-linear relationship (FIG. 3a), are used to construct an EP and a CP index[37] (FIG. 3b,c, respectively). CP El Niños have seemingly become more frequent than EP El Niños in recent decades[110] (FIG. 3b,c), most likely due to natural decadal climate variability[41,111,112].

Diversity of ENSO impact on SA

The aforementioned distinctions between CP and EP ENSO — specifically, the magnitude and location of SST anomalies — are important, given that they directly affect the depiction of ENSO impacts on SA, through both the tropical and extratropical pathways. Indeed, the climatic consequences of EP and CP ENSO can be profoundly different, in some extreme cases promoting opposite rainfall anomalies[35,38,39,42,113,114]. For example, during the 1997–98 EP El Niño, torrential rain inundated the coastal zone of Peru and Ecuador, while near-normal conditions prevailed for the 2015–16 event, which was a mix of an EP and CP El Niño[44,45,115] (FIG. 3b,c, stars). Here, we examine variability in EP and CP impacts through composites based on EP El Niño, CP El Niño, EP La Niña and CP La Niña events identified in FIG. 3b,c.

In all seasons, rainfall anomalies are stronger for EP El Niños compared with CP El Niños. Over SESA, for example, the positive summertime-rainfall anomalies are three times the magnitude for EP events when compared with CP events (FIG. 3d,e). These differences can be attributed to a more pronounced eastwards shift in the Walker circulation for EP El Niño events, resulting in descending motion and strengthened negative precipitation anomalies over north-east SA[38,41,42] (FIG. 3d,e). EP El Niños further tend to exhibit stronger and more well-defined PSA

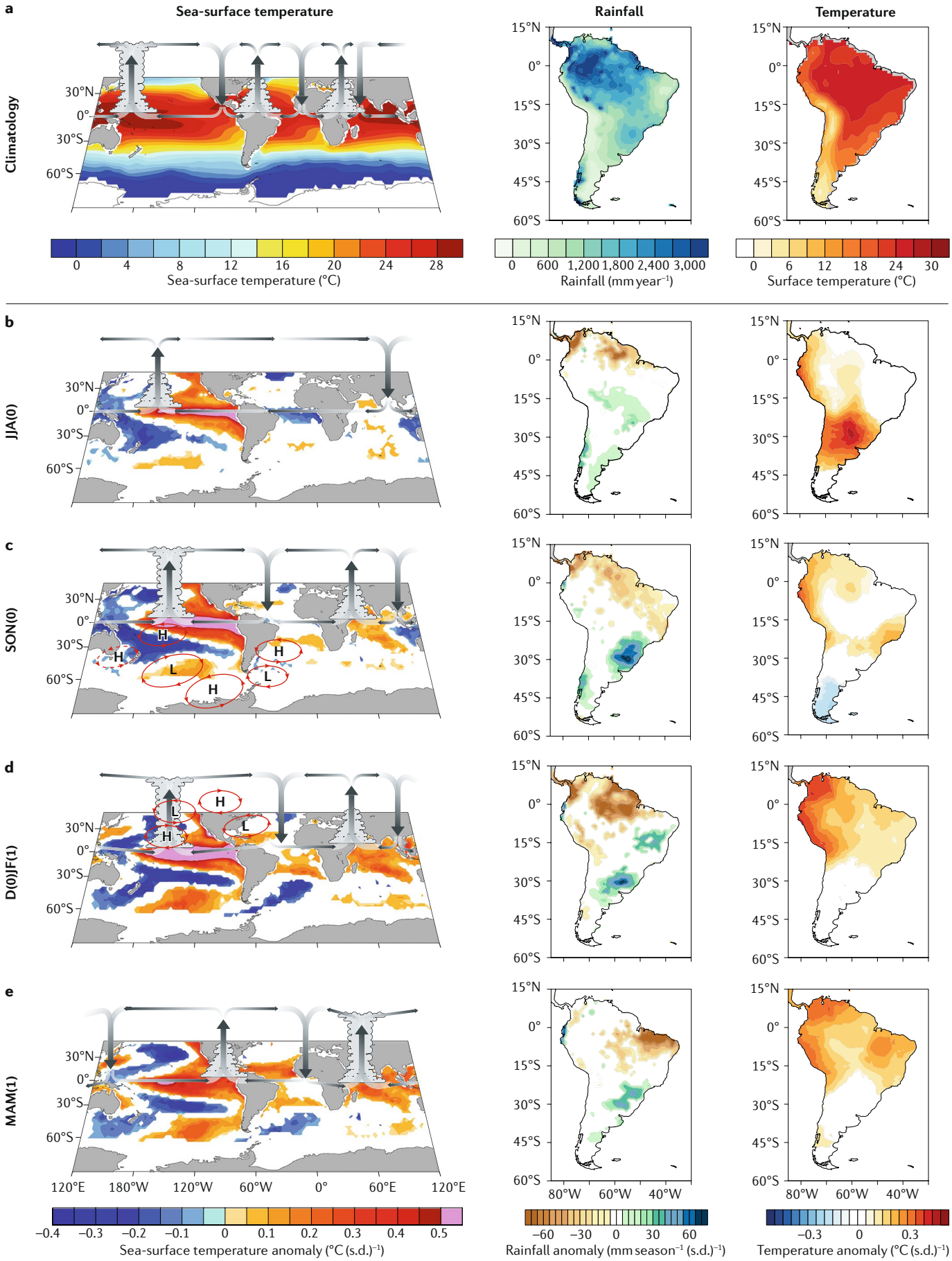
a
Sea-surface temperature
Rainfall
Temperature
Climatology
30°N
0°
30°S
60°S
15°N
0°
15°S
30°S
45°S
60°S
0 4 8 12 16 20 24 28
Sea-surface temperature (°C)
0 600 1,200 1,800 2,400 3,000
Rainfall (mm year⁻¹)
0 6 12 18 24 30
Surface temperature (°C)
b
JJA(0)
c
SON(0)
H
L
d
D(0)JF(1)
e
MAM(1)
120°E 180°W 120°W 60°W 0° 60°E 120°E
80°W 60°W 40°W
–0.4 –0.3 –0.2 –0.1 0 0.1 0.2 0.3 0.4 0.5
Sea-surface temperature anomaly (°C (s.d.)⁻¹)
–60 –30 0 30 60
Rainfall anomaly (mm season⁻¹ (s.d.)⁻¹)
–0.3 0 0.3
Temperature anomaly (°C (s.d.)⁻¹)

◀ Fig. 2 | **Evolution of a typical El Niño event and its impact on the South American climate.** Sea-surface temperature[192] (left), rainfall (middle) and surface-air temperature[191] (right) climatologies (part **a**) and El Niño–Southern Oscillation-related anomalies for June-July-August (JJA; part **b**), September-October-November (SON; part **c**), December-January-February (DJF; part **d**) and March-April-May (MAM; part **e**). Overlaid on the left panels is the Walker circulation, with upwards and downwards arrows reflecting rising and sinking branches, respectively. Climatologies are calculated over the period 1948–2016. Anomalies are calculated by regressing seasonally averaged variables on the normalized DJF Niño3.4 index, using data from the period 1948–2016. All values shown in the regression maps, in physical units per standard deviation (s.d.), are significant above the 90% confidence level. Year 0 in parentheses indicates an El Niño developing year and year 1 the subsequent decaying year. In SON (part **c**), the Pacific–South American teleconnection emerges, represented as a sequence of high-pressure (H) and low-pressure (L) systems from the central equatorial Pacific to the South Atlantic. In DJF (part **d**), a northwards teleconnection is found, the Pacific–North American pattern. The El Niño–Southern Oscillation's impact revolves around a prominent feature during an El Niño that includes an increase in rainfall along the west coast, accompanied by a dipole pattern of an anomalous dry condition in the north-east and wet condition in the south-east.

and PNA patterns[40–42,116]. Indeed, during CP El Niños, the PNA is relatively weak, producing minimal SST changes in the tropical North Atlantic (the Atlantic Meridional Mode) and, thereby, smaller rainfall anomalies in northern SA, especially during MAM[40,117,118] (FIG. 2e). Contrasts can further be related to SST warming along the western coast of SA during EP El Niños, which directly results in anomalously higher rainfall in Peru and Ecuador, a stronger SALLJ, transporting more moisture to SESA during JJA and SON during EP El Niño[38,41,42,92], and a strengthened blocking high to the west of the southern tip of SA during EP El Niño, increasing positive rainfall anomalies over central Chile[41].

CP La Niñas, by contrast, tend to exhibit a stronger and spatially coherent rainfall response than EP La Niñas (FIG. 3f,g), the latter of which are a relatively rare occurrence (FIG. 3b). For instance, excess rainfall over northern SA during DJF is much stronger, and during MAM more spatially coherent during CP La Niñas (FIG. 3f,g), owing to a stronger developing negative Atlantic Meridional Mode, which results in a more persistent southwards displacement of the ITCZ[35,42,119]. In some cases, though, La Niña events can be associated with drought over north-east Brazil, such as in 2011–12, when a positive Atlantic Meridional Mode overwhelmed the La Niña impact[35]. Moreover, negative SON rainfall anomalies in SESA also tend to be stronger for CP La Niñas compared with EP La Niñas associated with a stronger PSA, while in DJF, stronger rainfall deficits are observed in south-east Brazil[41], due to land surface–atmosphere interaction triggered by soil-moisture anomalies in the previous SON season[120] (FIG. 3g).

Thus, ENSO diversity directly affects the climatic impacts in SA. EP El Niños tend to have a stronger effect than CP El Niños, linked to the anomalous SST and convection. La Niña events further exhibit impacts with spatial patterns different from those of El Niño, with CP events typically stronger in intensity than their EP counterparts.

Modulation of ENSO impact

As well as being affected by the location, seasonality and sign of SST anomalies, ENSO's impact on SA is also modulated by local land surface–atmosphere interactions, air–sea interactions in the neighbourhood of the continent, other modes of interannual climate variability, inter-basin interactions and a changing mean climate, each of which is now discussed.

Land surface–atmosphere interactions

Local land surface–atmosphere interactions contribute to inter-event differences in ENSO climate impacts[120–122]. In northern SA, for example, soil moisture, evapotranspiration and rainfall recycling over the Amazon basin affect the response of the tropical North Atlantic to PNA teleconnections. Specifically, negative rainfall anomalies over the Amazon basin act to decrease the pressure gradient with the tropical North Atlantic, weakening the North Atlantic trade winds, in turn, warming SSTs[121,122], which inhibit the southwards movement of the Atlantic ITCZ and creating conditions unfavourable for rainfall in northern SA[121,122]. Thus, if the initial rainfall over the Amazon is lower than normal, it would reinforce the impact of the El Niño PNA teleconnections, leading to a further rainfall reduction in northern SA. Conversely, if the initial rainfall anomaly over the Amazon is positive, it would offset the impact of an El Niño[121,122].

A land surface–atmosphere feedback similarly explains an inverse relationship between antecedent SON and peak DJF rainfall in central-east SA during ENSO years[120]. For instance, a negative SON rainfall anomaly in central-east SA leads to low SON soil moisture and high late SON surface temperatures; this, in combination with topographical effects, enhances low-level anomalous convergence and cyclonic circulation over south-east Brazil, increasing moisture flux from the Atlantic, north-western SA and Amazon basin into central-east Brazil, thus, creating favourable conditions for increased rainfall in DJF. Conversely, an antecedent wet condition in SON leads to opposite anomalies in DJF. While this reversal of rainfall anomalies from spring to summer can also occur without the influence of the ENSO, it is more frequent during El Niño or La Niña years due to the rainfall anomalies it generates in central-eastern SA and because the ENSO teleconnection to this region is very weak in DJF[81,91,120]. Therefore, the effects of land surface–atmosphere feedback overcome those of ENSO remote forcing.

Neighbouring air–sea interactions

Air–sea interactions in the neighbourhood of the continent also have the potential to modulate ENSO impacts through either establishing anomalous rainfall on land[12,71,120] or altering the development of the ENSO itself[123]. For example, an El Niño-independent positive South Atlantic dipole mode — that is, anomalous cooling to the north-east South Atlantic and warming to the south-west — can shift the SACZ southwards and the ITCZ northwards[124], reinforcing El Niño-induced rainfall reductions over north-eastern SA. However, a positive South Atlantic dipole mode can itself be triggered by CP El Niño[116], presenting a positive feedback that intensifies the impact of the CP El Niño.

Interannual variability

The ENSO's impact on SA is also affected by other modes of variability.

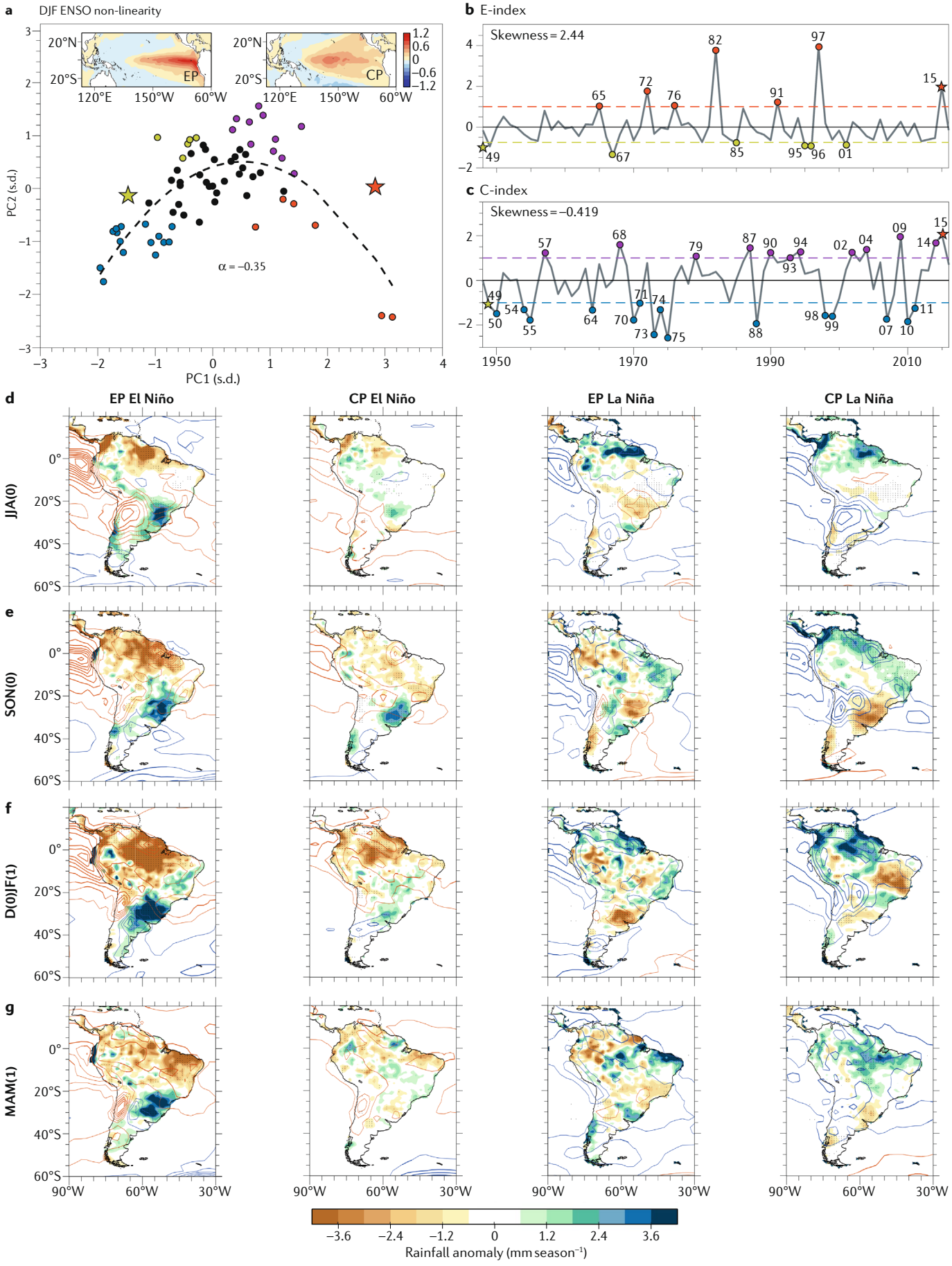
a
DJF ENSO non-linearity
20°N
20°S
EP
CP
120°E
150°W
60°W
1.2
0.6
0
−0.6
−1.2
PC2 (s.d.)
PC1 (s.d.)
α = −0.35
b E-index
Skewness = 2.44
c C-index
Skewness = −0.419
1950
1970
1990
2010
d
EP El Niño
CP El Niño
EP La Niña
CP La Niña
JJA(0)
e
SON(0)
f
D(0)JF(1)
g
MAM(1)
0°
20°S
40°S
60°S
90°W
60°W
30°W
−3.6
−2.4
−1.2
0
1.2
2.4
3.6
Rainfall anomaly (mm season⁻¹)

◀ Fig. 3 | **EP and CP ENSO regimes and their different impacts on the South American climate.** El Niño–Southern Oscillation (ENSO) non-linearity (α) represented by a quadratic relationship between the first and second principal components of December-January-February (DJF)-averaged sea-surface temperature anomalies[192] from 1948 to 2016 (REF.[37]) (part **a**). The eastern Pacific (EP) and central Pacific (CP) ENSO regimes can be described by an E-index $[(PC1 - PC2)/\sqrt{2}]$ (part **b**) and a C-index $[(PC1 + PC2)/\sqrt{2}]$ (part **c**), respectively, with their patterns shown in the insets in panel **a**. An EP El Niño is defined when the E-index is greater than 1.00 standard deviation (s.d.) (red circles in parts **a** and **b**) and an EP La Niña when the E-index is greater than −0.75 s.d. in amplitude (yellow circles in parts **a** and **b**). A CP El Niño or CP La Niña event is defined when the C-index exceeds 1 or −1 s.d. in amplitude, respectively (purple and blue circles in parts **a** and **b**). As EP La Niña is smaller in amplitude than CP La Niña, a threshold of 0.75 s.d. is used to maximize the number of events included. The red and yellow stars in parts **a**, **b** and **c** indicate the 2015–16 and 1949–50 events, which are mixed EP/CP El Niño and EP/CP La Niña, respectively. Composites of rainfall[190] (shading) and surface temperature[191] (contours) anomalies for EP El Niño (left), CP El Niño (middle-left), EP La Niña (middle-right) and CP La Niña (right) during June-July-August (JJA; part **d**), September-October-November (SON; part **e**), December-January-February (DJF; part **f**) and March-April-May (MAM; part **g**). Year 0 in parentheses indicates an El Niño developing year and year 1 the subsequent decaying year. Red and blue contours in parts **d**–**g** represent positive and negative surface-air-temperature anomalies, respectively, drawn at intervals of 0.2 °C. Thick contours or stippled areas indicate statistical significance above the 90% confidence level. EP El Niños generally have a stronger impact than CP El Niños, but can be opposite along the tropical west coast between EP and CP El Niños. Further, impacts of CP La Niñas are generally stronger than EP La Niñas, but the spatial pattern is not a mirror opposite of that associated with their respective El Niños.

North Atlantic SST variability. Although tropical North Atlantic SST responds to the ENSO-induced PNA teleconnection, the Atlantic Meridional Mode also operates independently from the Pacific[99,100] and can, therefore, offset or reinforce the impact of the PNA on the SST[33,34,40,99]. Moreover, the negative phase of the North Atlantic Oscillation — that is, anomalous low and high surface pressure in the northern mid-latitudes and high latitudes, respectively — reduces the north-easterly trades and SST in the tropical North Atlantic, leading to less rainfall in the Amazon basin[125] and Colombia[126].

Indian Ocean variability. The IOD[50] and the Indian Ocean basin-wide (IOB) warming[127] further act to offset or amplify the ENSO's impact on SA, specifically, as they tend to occur in conjunction with an El Niño event[128]. A positive phase of the IOD, characterized by an anomalous cooling in the east but warming in the western equatorial Indian Ocean in SON, can trigger Rossby wave trains similar to the PSA pattern during El Niño[52,129] (FIG. 4a), leading to increased rainfall in SESA and in central Chile by guiding weather systems (and, therefore, moisture) over the region[128]. IOB warming, a basin-wide warming that develops during the matured El Niño season of DJF and peaks in MAM, further triggers Rossby wave trains patterns similar to to those in SON and DJF, enhancing and prolonging the El Niño impact in SESA into MAM[127].

The SAM. The SAM is characterized by opposing geopotential-height anomalies between the mid-latitudes and high latitudes[47], a positive phase describing positive anomalies over the mid-latitudes and negative anomalies over the high latitudes, decreasing the strength of the mid-latitude westerlies and reducing the strength of high-latitude westerlies. A positive SAM produces drier conditions in SESA and central Chile, as the rain-bearing westerly systems are shifted polewards, which can offset or modulate the impact from an El Niño[51,130] (FIG. 4b). Indeed, while the SAM generally causes drying in SESA, El Niño events are typically conducive to rainfall[51], with the interplay between these two modes influencing the precipitation responses; during the 2015–16 El Niño, for example, negative rainfall anomalies predominated due to a strong offset by a positive SAM[130]. A similar situation was observed in central Chile, where the strong El Niño event was not able to break the prolonged drought affecting this region since 2010 because of the persistent positive SAM state[57]. In contrast, the positive SAM phase and the very strong El Niño during early 2016 conspired to produce an extreme drought that triggered severe environmental disruptions along western Patagonia because both lead to negative rainfall anomalies[131].

Decadal variability

In addition to the interannual variability, climatic impacts in SA also exhibit longer-term variability related to decadal variations in ENSO diversity and corresponding relationships with other modes of variability. For example, from the mid-1970s to late 1990s, when the IPO was positive (with anomalous cooling in the central and western regions of the North and South Pacific surrounded by warming along the equatorial and western coastline of the Americas), ENSO events included more occurrences of strong CP La Niña and strong EP El Niño events[132]. Since the 2000s, however, the IPO has been negative and ENSO events feature more CP El Niños, which are smaller in amplitude[110]. These decadal changes in ENSO characteristics act to modify the corresponding impacts in SA[53,133]. For instance, during the positive IPO, El Niño was associated with an increase in rainfall in southern Brazil and central Chile, a relationship that was not apparent during the negative IPO phase[55,57] (FIG. 4c). Furthermore, in Colombia, La Niña-induced rainfall is particularly large during the negative phase of the IPO, whereas El Niño-induced drying is exacerbated during the positive phase[134]. Further, ENSO–SAM and ENSO–IOD relationships also change on decadal timescales[130,135,136]. For instance, an El Niño, conducive to central Chile JJA rainfall, induces a negative SAM, which is also favourable to central Chile JJA rainfall, and this ENSO–SAM relationship, which reinforces the ENSO's impact on central Chile, has been weakening in recent decades[130,135]; similarly, an El Niño can induce a positive IOD, which reinforces El Niño-induced rainfall increase in SESA and in central Chile, but the El Niño and the IOD relationship has been weakening in recent decades[46]. These changes result in ENSO's impact on the South American climate becoming less robust in recent decades, and its prediction more challenging.

Inter-basin interactions

Since the year 2000, the warm phase of the Atlantic Multidecadal Variability has not only intensified the negative phase of the IPO[137] but also the two-way interaction between the tropical North Atlantic and the central equatorial Pacific, inducing a higher frequency of CP El Niños[138] (FIG. 3b,c). El Niño-induced warming of the

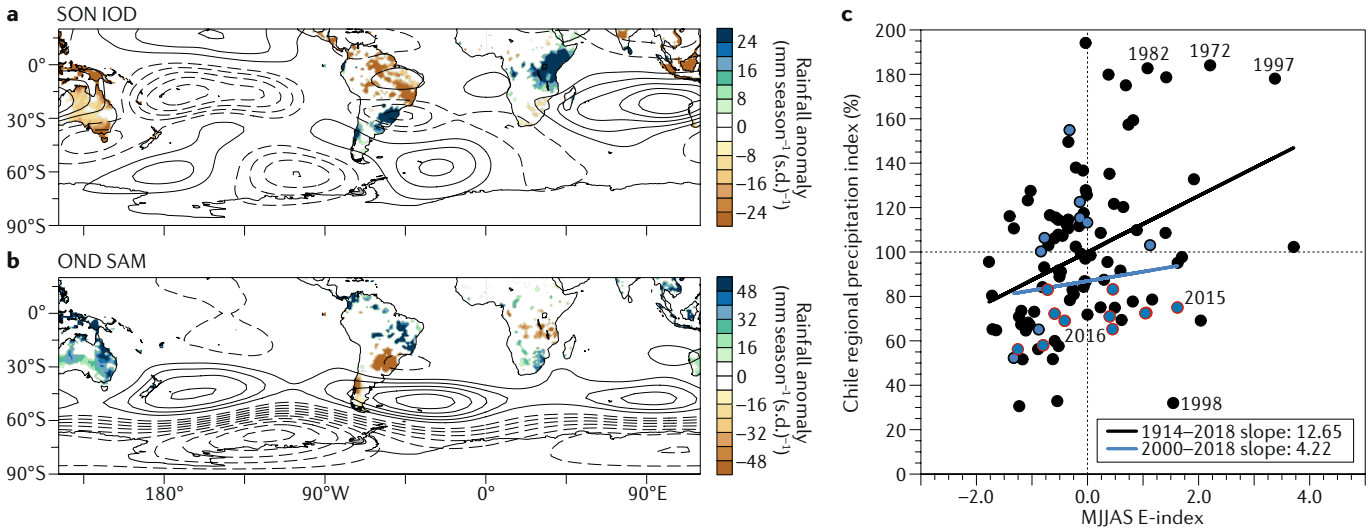

Fig. 4 | **Modulation of the ENSO's impact on SA. a** | Regression between September-November-October (SON) Indian Ocean Dipole (IOD)[50] and SON rainfall (shading) and 200-mb stream function (contours). Stream-function contours are drawn at intervals of 0.6 from −3 to 3 (10^6 m^2 s^{-1} (s.d.)$^{-1}$). **b** | Regression between October-November-December (OND) Southern Annular Mode (SAM)[58] with OND rainfall field (shading) and 200-mb geopotential height. Geopotential-height contours are drawn at intervals of 10 from −100 to 50 m (s.d.)$^{-1}$. Only values above the 90% confidence level are plotted. **c** | Relationship between May to September (MJJAS) E-index and central Chile regional precipitation index[57]. The black and blue lines show the regression for 1914–2018 and 2000–18, respectively. The red circles highlight the Chile megadrought years from 2009 to 2018. The diverse impact of the El Niño–Southern Oscillation (ENSO) on SA is modulated by a multitude of factors: the positive IOD, which tends to reinforce, and the positive SAM, which tends to offset, impacts from El Niño. ENSO's influence has been weakening, as indicated by the smaller slope in the recent period (blue line), which may contribute to the recent drought in central Chile. s.d., standard deviation.

tropical North Atlantic in MAM can initiate a La Niña in subsequent seasons[56], which is conducive to a cooling in the tropical North Atlantic in the following MAM, and vice versa. Recent North Atlantic background warming associated with a positive phase of the Atlantic Multidecadal Variability has intensified this inter-basin connection[49], leading to more frequent biennial CP El Niños[138], with an expected overall weaker impact on SA (FIG. 3d,e).

Warming climate

Recent evidence suggests that at least part of ENSO's impact on SA has already been impacted by greenhouse-warming-induced change. For example, the persistent positive SAM phase, as a result of Antarctic ozone depletion and increasing CO_2 (REF.[139]), may have contributed to a failure in the ENSO–rainfall teleconnection in central Chile and the megadrought in the region since 2010, and even the strong 2015–16 El Niño is not enough to compensate for these dry conditions[57] (FIG. 4c).

Implications

Understanding how ENSO impacts the climate of SA, including the variability and modulating factors, has important implications for seasonal and multi-year prediction, as well as for future projection of how the teleconnections may change in the future.

Predictions

The robustness of the local impacts in western SA associated with coastal El Niño or EP El Niño events and the tropical and extratropical teleconnection renders SA one of the regions where models demonstrate predictability in ENSO impact[140,141]. Given that EP El Niño is typically greater in amplitude than CP El Niño, and CP La Niña is greater in amplitude than EP cold anomalies, prediction of ENSO types is, in principle, expected to enhance prediction of the corresponding impact from a signal-to-noise-ratio perspective. For example, since the early 2000s, there has been a general reduction in ENSO predictability[142], which might be associated with more CP ENSO. However, whether an ENSO impact emerges depends on a number of factors, including the evolution of ENSO itself[38] and the impact of other modes of climate variability[33,34,140]. For example, the prediction of north-east Brazil rainfall relies more on a north-minus-south SST gradient in the tropical Atlantic than on Pacific SST anomalies[99]. More specifically, a positive interhemispheric SST gradient anomaly during El Niño keeps the ITCZ in the tropical North Atlantic, which, in turn, leads to rainfall deficits over north-east Brazil, and vice versa for La Niña[143]. This relationship emerges because the Atlantic meridional SST gradient and the position of the ITCZ are not solely driven by the ENSO but are also affected by ocean and atmosphere dynamics within the South Atlantic via, for example, Atlantic Niños[34] and variations in the Benguela upwelling system[144]. Thus, predictors incorporating both the tropical Pacific and Atlantic SSTs result in improved prediction compared with that achieved when using SSTs from either ocean alone[35,145].

Both the Indian and the Atlantic oceans feed back into the Pacific, which provides additional precursors for the prediction of ENSO diversity and, therefore, its impact. A positive IOD not only reinforces the development of a concurrent El Niño by promoting anomalous westerlies in the western Pacific but also intensifies an El Niño-induced IOB warming in DJF and MAM[46] and accelerates the transition to a La Niña event[47]. Likewise,

La Niña events can be triggered by an El Niño-induced anomalous warming in the tropical North Atlantic in MAM[56,138] or an Atlantic Niño in JJA[146]. Thus, incorporating information of oceans outside the Pacific can potentially improve the prediction of ENSO diversity[46,138,147], evolution and phase transition[56], as demonstrated in hindcast experiments[46,56,147–149], ultimately providing more accurate information for seasonal predictions in SA. The Indian and Atlantic feedback to the Pacific also operates on decadal timescales, enhancing multi-year prediction[147,150]. For example, a decadal warming trend in the tropical Atlantic leads to a cooling trend in the Pacific[137].

Projection of the South American mean climate

Under greenhouse warming, the majority of climate models project a mean pattern of rainfall change somewhat similar to the anomaly pattern associated with an El Niño[151–153]. This pattern includes an increase in SON and DJF rainfall over SESA[153] and a likely reduction in the central-eastern Amazon and north-east Brazil regions[151,154,155]. One exception is central Chile, where most climate models predict decreased precipitation, contrasting with the wetter-than-normal conditions associated with an El Niño. However, the extent of the projected change depends on model realisms in simulating ENSO.

The ability of models to simulate ENSO diversity and non-linearity can be assessed in terms of the dynamical non-linear coefficient |α| (FIG. 3a), diagnosed over the modelled 1900–2099 period (FIG. 5a). Models simulating an |α| close to zero indicate that the first and second PCs are not able to simulate the observed ENSO non-linearity and diversity. With a realistic |α|, the pattern associated with PC1 represents the average pattern of all ENSO events, and the pattern associated

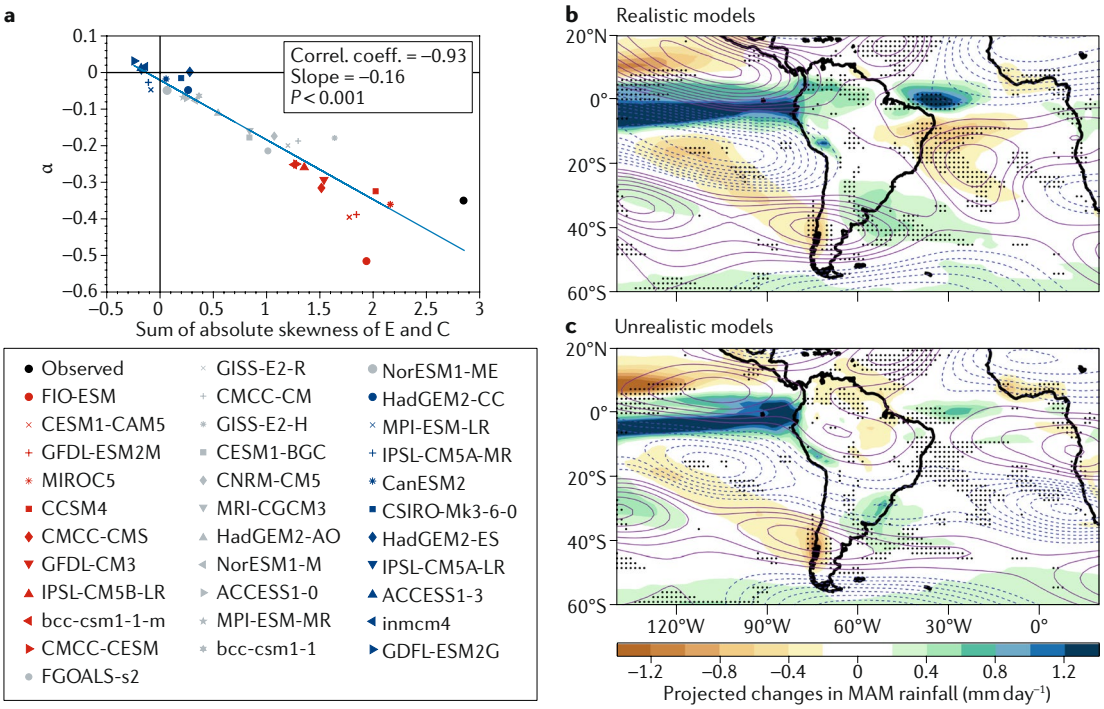

Fig. 5 | **Dependence of projected rainfall change on the level of simulated ENSO non-linearity.** Relationship between α, a greater amplitude of which means that a model's ability to produce distinct central Pacific and eastern Pacific El Niño–Southern Oscillation (ENSO) systems is higher, and the sum of absolute skewness of the E-index (positive skewness) and C-index (negative skewness) across all CMIP5 models. A positive skewness of the E-index means that warm anomalies are able to grow to a greater amplitude than cold anomalies, as shown in FIG. 3b (part **a**). An |α| close to zero suggests that the first and second principal components (PCs) are not non-linearly linked, which is opposite to the observed (black circle). A substantial |α| indicates that the pattern associated with PC1 is the average pattern of El Niño anomalies, and the pattern associated with PC2 modulates the PC1 pattern to produce the difference between central Pacific and eastern Pacific El Niño events, and the asymmetry between El Niño and La Niña, as shown in FIG. 3a. Models are separated into two different groups: realistic models (red symbols), which represent the best ten models that simulate |α|, and unrealistic models (blue symbols), which represent the worst ten models. Other models are indicated in grey. Multi-model ensemble mean of projected changes in rainfall during March-April-May (MAM) between the 2000–99 and the 1900–99 periods forced under RCP8.5 (REF.[193]) using the realistic models (part **b**) and less realistic models (part **c**). The contours reflect the projected change in stream function at 200 mb, with the solid purple and dashed blue lines indicating positive and negative stream-function anomalies, respectively; contours are drawn at intervals of 0.2×10^6. The dotted areas in parts **b** and **c** indicate a statistically significant difference between realistic and less realistic models at the 90% confidence level using a Student's *t*-test. Models that simulate stronger ENSO non-linearity project a rather different future from models simulating weaker ENSO non-linearity, including an increase in the mean rainfall in the northern Amazon basin and drier conditions south of the Nordeste.

with PC2 modulates the PC1 pattern to produce the difference between weak and strong El Niño events, and the asymmetry between El Niño and La Niña (FIG. 3a). These so-called realistic models — that is, the ten models with |α| closest to that observed — can be used to examine projected rainfall changes. In the realistic models, the distinction between EP and CP ENSO are clearer, ENSO diversity is higher and its response to greenhouse warming is stronger; in particular, when compared with the unrealistic models, the projected increase in strong EP El Niño and strong La Niña is greater[106] and mean SSTs in the eastern equatorial Pacific are warmer[156]. Consequently, an increasing MAM rainfall trend in the Amazon and a subdued MAM drying trend in southern Chile are projected in the realistic models (FIG. 5b,c), related to increased rainfall linked directly to warmer mean SSTs in the eastern equatorial Pacific[156], which offsets a SAM-related rainfall reduction in the central Chile region. The increase in mean rainfall in the northern Amazon basin, and the drier conditions south of the Nordeste, are also stronger in those models, simulating stronger ENSO non-linearity (FIG. 5b,c).

In addition, models that simulate a stronger decadal Atlantic feedback to the Pacific, in which the cooling effect induced by the Atlantic warming is greater, project a smaller warming in the Pacific[49] and, likely, smaller rainfall changes in SA. These changes suggest that the source of uncertainty in the projected rainfall change and future ENSO impact on the South American climate is not limited to the realism of the ENSO and Pacific conditions in climate models.

Projection of ENSO teleconnections

At present, there is no evidence to suggest that the contemporary pathways through which ENSO influences SA are likely to change under greenhouse warming[157–159]. However, given that strong El Niño[106] and strong La Niña[160] events are projected to increase in frequency, ENSO-related climate and weather extremes are likely to increase in most regions of SA. Further, the frequency of coastal El Niño events is projected to increase with climate change[25,161]. As such, regions with a robust ENSO signal in the current climate are generally expected to experience an increase in ENSO-driven extreme events in the future[162], as the impact superimposes on the mean state change[163].

In terms of whether the intensity of the ENSO teleconnection will change, previous studies using historical Niño indices show either a weakened teleconnection[157,158] or no robust change in ENSO teleconnection patterns[164,165]. However, the projected change is likely to depend on each model's ability to simulate ENSO diversity and non-linearity[106] (FIG. 6). For instance, in models that simulate a higher level of ENSO diversity, a weaker drying in north-western SA and a broader and more intense rainfall increase in SESA in SON is projected (FIG. 6b,c). Nevertheless, CP or EP ENSO SST anomaly patterns differ vastly from one model to another, even in models that simulate ENSO diversity[106], which remains a source of uncertainty for simulating and projecting ENSO's regional impacts over SA.

Even if the mechanisms for ENSO impacts do not change, ENSO impact is likely to be modified by the mean state changes. Positive temperature anomalies during El Niño on a warmer climate could lead to deadly heat in the Amazon region and tropical western SA[166]. In addition to the dipole-like rainfall change, the mean SACZ is likely to move southwards, as observed since 1979 (REF.[167]). On the other hand, the projected positive SAM trend is likely to decrease the mean rainfall in central Chile, offsetting an El Niño-induced rainfall increase[57]. The projected reduction in rainfall and soil moisture in the Amazon region may exacerbate, via increased evaporation, higher temperatures and less land-rainfall recycling[168], and the impacts of El Niño-driven drought conditions, conducive to more extreme fire risk[162].

Summary and pathways forwards

How ENSO impacts SA would, at first sight, appear to be a relatively simple and solved problem; the tendency of floods and droughts along the tropical west coast of Ecuador/Peru and Colombia, respectively, during strong or coastal El Niños has long been known. The more comprehensive picture, such as droughts in the Amazon and floods in SESA during El Niños, has also been familiar to many. However, ENSO's impact on SA is dependent on a multitude of factors, including ENSO diversity, the impact from other modes of climate variability and inter-basin interactions, especially between the Pacific and the Atlantic. CP and EP ENSO events, for example, can have opposite impacts or disparate impacts, related to contrasting teleconnection efficiencies via the tropical and extratropical pathways. For instance, in the west coastal fringe, the tendency of floods may not occur during a CP El Niño and, instead, drier than normal conditions can be prevalent. Modes of variability in the Indian and Atlantic oceans further feed back into the Pacific, affecting ENSO properties, and, thereby, modulating the resulting impacts in SA. A positive IOD, for instance, favours the development of an El Niño, and a positive Atlantic Meridional Mode during MAM can trigger a CP La Niña[56,138], in turn, promoting anomalous climatic patterns typical of those events. These modes of climate variability can also modify ENSO impacts directly, either reinforcing corresponding anomalies (such as when an El Niño occurs in conjunction with a positive IOD[129]) or muting them (for central Chile, such as when an El Niño occurs concurrently with a positive SAM). Moreover, decadal-scale variability — both in regards to ENSO and the resulting interactions with other modes — adds a further complication to diagnosing ENSO teleconnections, especially in light of the relatively short instrumental record.

ENSO thus represents an important, yet complicated, influence on SA, promoting temperature and precipitation anomalies that have profound socio-economic, ecological and environmental impacts. Therefore, it is vital to reduce the uncertainties in ENSO in both contemporary and future climates, which can be achieved through continued palaeoclimate investigations, model developments and targeted research.

Extending the instrumental record further back in time by using palaeoclimate proxies can help decipher the complexity of ENSO impacts on SA. At the same

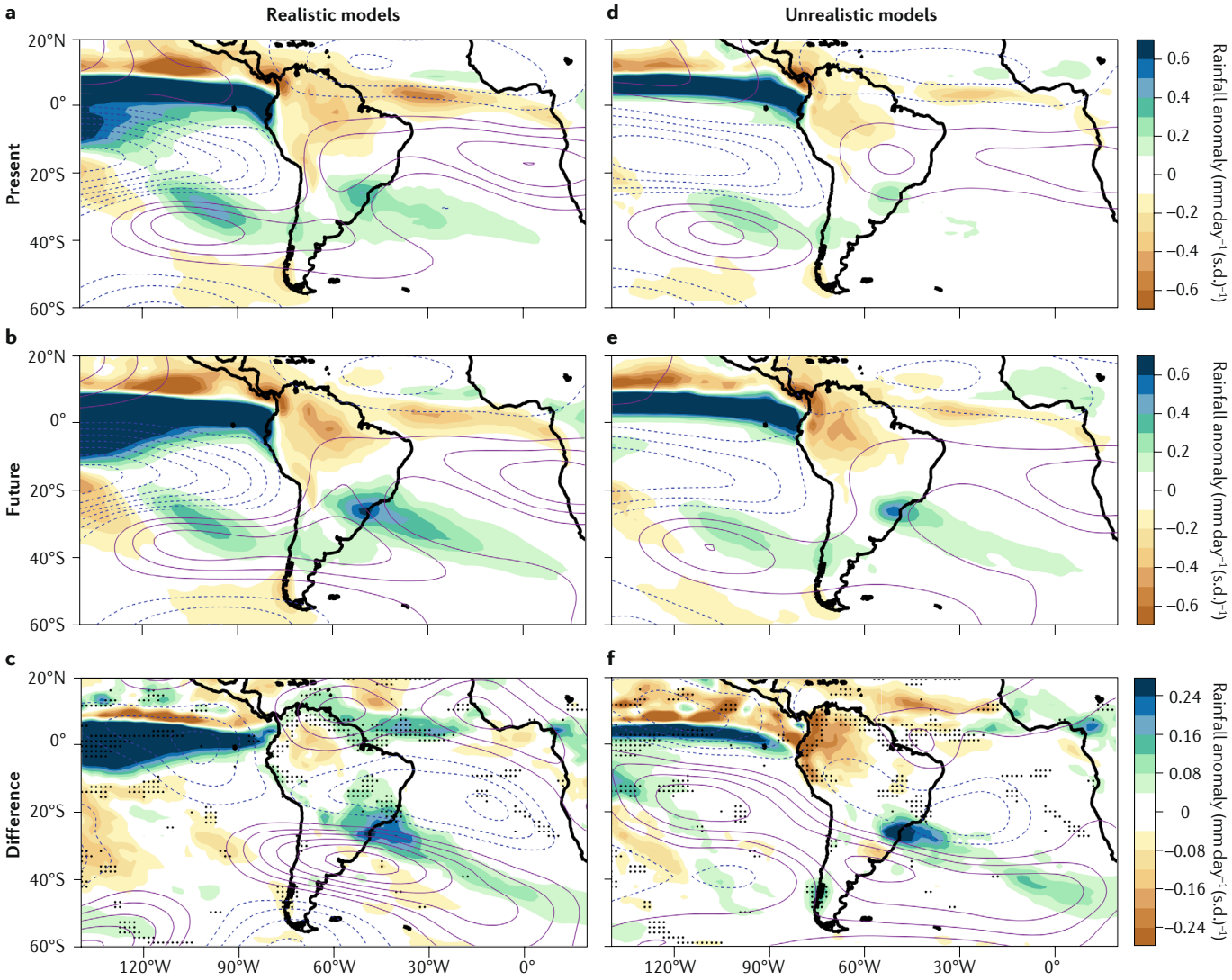

Fig. 6 | **Dependence of EP ENSO teleconnection on simulated ENSO non-linearity.** Multi-model ensemble mean of eastern Pacific (EP) El Niño–Southern Oscillation (ENSO) teleconnections during September-October-November (SON), as simulated by the realistic models (red symbols in FIG. 5a) for the present climate (1900–99; part **a**), future climate (2000–99; part **b**) and the difference (part **c**), and by the unrealistic models (blue symbols in FIG. 5a) for the present climate (1900–99; part **d**), future climate (2000–99; part **e**) and the difference (part **f**). Rainfall (shading) and 200-mb stream function (contours) anomalies are calculated by regressing SON-averaged values onto the SON E-index prior to multi-model averaging. The solid purple and dashed blue lines indicate positive and negative stream-function anomalies, respectively; contours are drawn at intervals of 0.5×10^6 for parts **a**, **b**, **d** and **e**, and 0.15×10^6 for parts **c** and **f**. The dotted areas in **c** and **f** reflect statistically significant differences at the 90% confidence level using a Student's *t*-test. The detailed structure of the projected changes between the two groups is different, but both show a tendency for a strengthened teleconnection. Further, relative to the unrealistic models, teleconnection patterns associated with a positive E-index feature less drying along the tropical west coast in the present-day and future climate and in the projected change in realistic models.

time, palaeoproxies can improve understanding of ENSO's response to past external climate forcing, such as changes in the Earth's orbit and volcanic eruptions. In fact, it was iconic records from SA, such as sediment cores from Laguna Parcacocha in Ecuador[169,170] and El Junco in the Galápagos[171], that motivated palaeoclimate modelling of past ENSO behaviour[172]. These records show, for instance, a decrease in ENSO variance during the mid-Holocene (4–7 ka before present) and a ramp-up in the past 3,000 years. However, the occurrence of extreme rainfall in northern SA heavily depends on ENSO diversity, which needs to be taken into account[173]. Despite the complexity of ENSO impacts on SA, it remains a prime location for palaeoclimate proxy collection and analysis, providing insights into how ENSO and its impacts have changed in the past and guiding studies of how ENSO may change in the future. Extending such proxy record further back to the early Holocene when atmospheric CO_2 was decreasing would provide a more complete picture of ENSO response in the past.

Climate models provide a vital tool for understanding past and projecting future ENSO impacts, but they suffer from long-standing systematic errors. These include a cold bias in the equatorial CP[174,175] and the equatorial eastern Indian Ocean[176], but a warm bias in the eastern boundary-current-system regions, including the tropical Pacific and Atlantic[48,177]. The cold-tongue bias could have

a substantial impact on the simulated characteristics of ENSO and the IOD[178], and the bias in the Atlantic could be responsible for the weak Atlantic–Pacific interaction. Other model errors include unrealistic ENSO seasonal phase locking[179], which can affect the timing of ENSO impact on SA, weak ENSO diversity and the associated impacts[106,156,165,179]. It is not clear whether these errors are related to, for instance, unrealistic representation of land-surface processes[180], a dry bias in the central Amazonia[181] and Northern American regions[182], a wet bias in the vicinity of the Andes[183] or low variability in the SACZ and in ENSO-induced extratropical Rossby wave trains[51].

Thus, there is considerable uncertainty in the projected change in ENSO impact on SA. Under greenhouse warming, models that simulate a more realistic ENSO diversity tend to produce a stronger increase in CP and EP ENSO variability than those that do not[106], suggesting that the ENSO impact on SA could be more extreme in the future. But the pattern and its projected mean state change could be substantially different if model systematic errors in Atlantic–Pacific interactions and in ENSO diversity are corrected[49]. Given that the systematic errors in the tropical Atlantic have persisted for many model generations and may take a long time to rectify, flux adjustments in climate models can be a useful approach for exploring the Atlantic–Pacific interactions in the current climate and for gauging their impact on future change under differing climate-change-forcing scenarios.

Recent progress in our understanding of ENSO impact on SA provides valuable guidance for setting research priorities. Among these is the urgent need to reduce model systematic errors, like those associated with the ocean–atmosphere processes in the EP, because of their adverse impacts on the skill of seasonal forecasts and future projections. Given the models' inability to reproduce the land-surface process responsible for the inverse relationship between SON and DJF rainfall in central-east SA[184], strengthened effort in understanding the associated processes is in order, so that these are represented as accurately as possible in models. Further, comprehensive studies of how climate change interacts with ENSO impacts are required if we are to fully grasp the consequences. Finally, there is a need for higher spatial and temporal resolution to capture the details of ENSO impacts embedded in the SA rainfall dipole pattern. This pattern results from both tropical and extratropical teleconnections, which are mediated by weather events on daily to intra-seasonal timescales[185,186]. Some of these weather events are extreme and it is these extreme events that are most consequential in terms of socio-economic impacts (BOX 1). Importantly, it has been suggested that these ENSO-related extreme events are already being amplified by underlying climate-change trends, as, for example, in the heightened risk of Amazon fires during the 2015–16 El Niño[187].

Scientific progress on these issues will not only be of benefit to SA but to the world as well. Ocean–atmosphere–land interactions that affect the climate of the Amazon feed back into the global climate[21,188,189]. In a globalized world, economic impacts felt in SA ripple through international markets, especially for weather-sensitive and climate-sensitive commodities. Ultimately, progress in understanding, assessing and predicting ENSO's impact on SA and its global consequences will depend critically on sustained global ocean and climate observations, more comprehensive palaeoreconstructions and climate-model improvements.

Published online 10 April 2020

1. McPhaden, M. J., Zebiak, S. E. & Glantz, M. H. ENSO as an integrating concept in Earth science. *Science* **314**, 1740–1745 (2006).
2. Bjerknes, J. A possible response of the atmospheric Hadley circulation to equatorial anomalies of ocean temperature. *Tellus* **18**, 820–829 (1966).
3. Bjerknes, J. Atmospheric teleconnections from the equatorial Pacific. *Mon. Weather Rev.* **97**, 163–172 (1969).
4. Carrillo, C. N. Disertación sobre las corrientes y estudios de la corriente Peruana de Humboldt. *Bol. Soc. Geogr. Lima* **11**, 72–110 (1892).
5. Aceituno, P. On the functioning of the Southern Oscillation in the South American sector. Part I: surface climate. *Mon. Weather Rev.* **116**, 505–524 (1988).
6. Rao, V. B. & Hada, K. Characteristics of rainfall over Brazil: annual variations and connections with the Southern Oscillation. *Theor. Appl. Climatol.* **42**, 81–91 (1990).
7. Grimm, A. M., Ferraz, S. E. & Gomes, J. Precipitation anomalies in southern Brazil associated with El Niño and La Niña events. *J. Clim.* **11**, 2863–2880 (1998).
8. Grimm, A. M., Barros, V. R. & Doyle, M. E. Climate variability in southern South America associated with El Niño and La Niña events. *J. Clim.* **13**, 35–58 (2000).
Offers a comprehensive view of the precipitation and circulation anomalies associated with the various stages of El Niño and La Niña events over southern South America.
9. Barros, V. R., Grimm, A. M. & Doyle, M. E. Relationship between temperature and circulation in southeastern South America and its influence from El Niño and La Niña events. *J. Meteorol. Soc. Jpn. Ser. II* **80**, 21–32 (2002).
10. Ropelewski, C. F. & Halpert, M. S. Global and regional scale precipitation patterns associated with the El Niño/Southern Oscillation. *Mon. Weather Rev.* **115**, 1606–1626 (1987).
11. Ropelewski, C. F. & Halpert, M. S. Precipitation patterns associated with the high index phase of the Southern Oscillation. *J. Clim.* **2**, 268–284 (1989).
12. Takahashi, K. & Martínez, A. G. The very strong coastal El Niño in 1925 in the far-eastern Pacific. *Clim. Dyn.* **52**, 7389–7415 (2019).
13. Rasmusson, E. M. & Carpenter, T. H. Variations in tropical sea surface temperature and surface wind fields associated with the Southern Oscillation/El Niño. *Mon. Weather Rev.* **110**, 354–384 (1982).
14. Anderson, W. B., Seager, R., Baethgen, W., Cane, M. & You, L. Synchronous crop failures and climate-forced production variability. *Sci. Adv.* **5**, eaaw1976 (2019).
15. Lehodey, P. et al. Climate variability, fish, and fisheries. *J. Clim.* **19**, 5009–5030 (2006).
16. Bouma, M. J. et al. Predicting high-risk years for malaria in Colombia using parameters of El Niño Southern Oscillation. *Trop. Med. Int. Health* **2**, 1122–1127 (1997).
17. Poveda, G. et al. Coupling between annual and ENSO timescales in the malaria-climate association in Colombia. *Environ. Health Perspect.* **109**, 489–493 (2001).
Provides evidence that the El Niño phenomenon intensifies the annual cycle of malaria cases in endemic areas of Colombia as a consequence of concomitant anomalies in the normal annual cycle of temperature and precipitation.
18. Aragão, L. E. O. C. et al. 21st Century drought-related fires counteract the decline of Amazon deforestation carbon emissions. *Nat. Commun.* **9**, 536 (2018).
19. Poveda, G., Jaramillo, A., Gil, M. M., Quiceno, N. & Mantilla, R. Seasonality in ENSO related precipitation, river discharges, soil moisture, and vegetation index (NDVI) in Colombia. *Water Resour. Res.* **37**, 2169–2178 (2001).
20. Acevedo, E. C., Turbay, S., Hurlbert, M., Barco, M. H. & Lopez, K. J. Governance and climate variability in Chinchiná River, Colombia. *Int. J. Clim. Change Strateg. Manag.* **8**, 632–653 (2016).
21. Jiménez-Muñoz, J. C. et al. Record-breaking warming and extreme drought in the Amazon rainforest during the course of El Niño 2015–2016. *Sci. Rep.* **6**, 33130 (2016).
22. Malhi, Y. et al. Climate change, deforestation, and the fate of the Amazon. *Science* **319**, 169–172 (2008).
23. Marengo, J. A. et al. Climatic characteristics of the 2010–2016 drought in the semiarid Northeast Brazil region. *An. Acad. Bras. Cienc.* **90**, 1973–1985 (2018).
24. Takahashi, K. et al. The 2017 coastal El Niño [in State of the Climate in 2017]. *Bull. Am. Meteorol. Soc.* **99**, S210–S211 (2018).
25. Peng, Q., Xie, S. P., Wang, D., Zheng, X. T. & Zhang, H. Coupled ocean-atmosphere dynamics of the 2017 extreme coastal El Niño. *Nat. Commun.* **10**, 298 (2019).
26. Grimm, A. M. & Tedeschi, R. G. ENSO and extreme rainfall events in South America. *J. Clim.* **22**, 1589–1609 (2009).
27. Tachini, M. *Flood Damage Assessment in the Municipality of Blumenau* (in Portuguese). Doctoral thesis, Federal Univ. Santa Catarina, 179 pp (2010).
28. ONEMI. *Annual Summary of Natural Hazards and Emergencies*. Technical report, Oficina Nacional de Emergencias, Chile. 53 pp (1997).

29. Aldunce Ide, P. & González, M. Desastres asociados al clima en la agricultura y medio rural en Chile. Departamento de Ciencias Ambientales y Recursos Naturales Renovables, Facultad de Ciencias Agronómicas, Universidad de Chile; Fundación para la Innovación Agraria (FIA), Ministerio de Agricultura (2009).
30. Quinn, W. H., Neal, V. T. & De Mayolo, S. E. A. El Niño occurrences over the past four and a half centuries. *J. Geophys. Res. Oceans* **92**, 14449–14461 (1987).
Documents El Niño occurrences over a multi-century period based on evidence from the west coast region of northern South America and its adjacent Pacific Ocean waters.
31. Meggers, B. J. Archeological evidence for the impact of mega-Niño events on Amazonia during the past two millennia. *Clim. Change* **28**, 321–338 (1994).
32. Czaja, A. & Frankignoul, C. Observed impact of Atlantic SST anomalies on the North Atlantic Oscillation. *J. Clim.* **15**, 606–623 (2002).
33. Giannini, A., Saravanan, R. & Chang, P. The preconditioning role of tropical Atlantic variability in the development of the ENSO teleconnection: implications for the prediction of Nordeste rainfall. *Clim. Dyn.* **22**, 839–855 (2004).
34. Chang, P., Fang, Y., Saravanan, R., Ji, L. & Seidel, H. The cause of the fragile relationship between the Pacific El Niño and the Atlantic Niño. *Nature* **443**, 324–328 (2006).
35. Rodrigues, R. R. & McPhaden, M. J. Why did the 2011–2012 La Niña cause a severe drought in the Brazilian Northeast? *Geophys. Res. Lett.* **41**, 1012–1018 (2014).
36. Ashok, K., Behera, S. K., Rao, S. A., Weng, H. & Yamagata, T. El Niño Modoki and its possible teleconnection. *J. Geophys. Res. Oceans* **112**, C11007 (2007).
37. Takahashi, K., Montecinos, A., Goubanova, K. & Dewitte, B. ENSO regimes: Reinterpreting the canonical and Modoki El Niño. *Geophys. Res. Lett.* **38**, L10704 (2011).
Provides independent indices that differentiate central and eastern Pacific El Niño events and the asymmetry with their La Niña counterparts.
38. Hill, K. J., Taschetto, A. S. & England, M. H. South American rainfall impacts associated with inter-El Niño variations. *Geophys. Res. Lett.* **36**, L19702 (2009).
39. McPhaden, M. J. Evolution of the 2002/03 El Niño. *Bull. Am. Meteorol. Soc.* **85**, 677–695 (2004).
Describes the contrasting rainfall anomalies in the coastal zone of western South America associated with the 2002–03 El Niño (a central Pacific event) and the 1997–98 El Niño (an eastern Pacific event).
40. Rodrigues, R. R., Haarsma, R. J., Campos, E. J. D. & Ambrizzi, T. The impacts of inter-El Niño variability on the tropical Atlantic and northeast Brazil climate. *J. Clim.* **24**, 3402–3422 (2011).
41. Tedeschi, R. G., Grimm, A. M. & Cavalcanti, I. F. Influence of Central and East ENSO on extreme events of precipitation in South America during austral spring and summer. *Int. J. Climatol.* **35**, 2045–2064 (2015).
Outlines the magnitude and geographic variability of precipitation anomalies in South America associated with central Pacific and eastern Pacific El Niño and La Niña events.
42. Tedeschi, R. G., Grimm, A. M. & Cavalcanti, I. F. Influence of Central and East ENSO on precipitation and its extreme events in South America during austral autumn and winter. *Int. J. Climatol.* **36**, 4797–4814 (2016).
43. McPhaden, M. J. Playing hide and seek with El Niño. *Nat. Clim. Change* **5**, 791–795 (2015).
44. L'Heureux, M. L. et al. Observing and predicting the 2015/16 El Niño. *Bull. Am. Meteorol. Soc.* **98**, 1363–1382 (2017).
45. Santoso, A., McPhaden, M. J. & Cai, W. The defining characteristics of ENSO extremes and the strong 2015/2016 El Niño. *Rev. Geophys.* **55**, 1079–1129 (2017).
46. Izumo, T. et al. Influence of the state of the Indian Ocean Dipole on the following year's El Niño. *Nat. Geosci.* **3**, 168–172 (2010).
47. Kug, J.-S. & Kang, I.-S. Interactive feedback between ENSO and the Indian Ocean. *J. Clim.* **19**, 1784–1801 (2006).
Suggests that an anomalous warming in the Indian Ocean produces an easterly wind anomaly over the western Pacific, which helps termination of an El Niño and its transition to La Niña.
48. Kucharski, F., Syed, F. S., Burhan, A., Farah, I. & Gohar, A. Tropical Atlantic influence on Pacific variability and mean state in the twentieth century in observations and CMIP5. *Clim. Dyn.* **44**, 881–896 (2015).
49. Cai, W. et al. Pantropical climate interactions. *Science* **363**, eaav4236 (2019).
50. Saji, N. H., Goswami, B. N., Vinayachandran, P. N. & Yamagata, T. A dipole mode in the tropical Indian Ocean. *Nature* **401**, 360–363 (1999).
51. Vera, C. S. & Silvestri, G. Precipitation interannual variability in South America from the WCRP-CMIP3 multi-model dataset. *Clim. Dyn.* **32**, 1003–1014 (2009).
52. Saji, N. H., Ambrizzi, T. & Ferraz, S. E. T. Indian Ocean Dipole mode events and austral surface air temperature anomalies. *Dyn. Atmos. Oceans* **39**, 87–101 (2005).
53. Andreoli, R. V. & Kayano, M. T. ENSO-related rainfall anomalies in South America and associated circulation features during warm and cold Pacific decadal oscillation regimes. *Int. J. Climatol.* **25**, 2017–2030 (2005).
54. Kayano, M. T. & Capistrano, V. B. How the Atlantic multidecadal oscillation (AMO) modifies the ENSO influence on the South American rainfall. *Int. J. Climatol.* **34**, 162–178 (2014).
55. Fernandes, L. G. & Rodrigues, R. R. Changes in the patterns of extreme rainfall events in southern Brazil. *Int. J. Climatol.* **38**, 1337–1352 (2018).
56. Ham, Y.-G., Kug, J.-S., Park, J.-Y. & Jin, F.-F. Sea surface temperature in the north tropical Atlantic as a trigger for El Niño/Southern Oscillation events. *Nat. Geosci.* **6**, 112–116 (2013).
57. Garreaud, R. D. et al. The Central Chile Mega Drought (2010–2018): a climate dynamics perspective. *Int. J. Climatol.* **39**, 421–439 (2019).
58. Gong, D. & Wang, S. Definition of Antarctic oscillation index. *Geophys. Res. Lett.* **26**, 459–462 (1999).
59. Power, S., Casey, T., Folland, C., Colman, A. & Mehta, V. Inter-decadal modulation of the impact of ENSO on Australia. *Clim. Dyn.* **15**, 319–324 (1999).
60. Levine, A. F. Z., McPhaden, M. J. & Frierson, D. M. W. The impact of the AMO on multidecadal ENSO variability. *Geophys. Res. Lett.* **44**, 3877–3886 (2017).
61. Garreaud, R. D., Vuille, M., Compagnucci, R. & Marengo, J. Present-day South American Climate. *Palaeogeogr. Palaeoclimatol. Palaeoecol.* **281**, 180–195 (2009).
62. Poveda, G., Waylen, P. R. & Pulwarty, R. Modern climate variability in northern South America and southern Mesoamerica. *Palaeogeogr. Palaeoclimatol. Palaeoecol.* **234**, 3–27 (2006).
63. Montoya, G., Pelkowski, J. & Eslava, J. A. On the northeastern trade winds and the existence of a low-level jet over the piedmont of the Eastern Andes [in Spanish]. *Rev. Acad. Colomb. Cienc.* **25**, 363–370 (2001).
64. Poveda, G. & Mesa, O. J. The CHOCO low-level jet and two other jets over Colombia: climatology and variability during ENSO [in Spanish]. *Rev. Acad. Colomb. Cienc.* **23**, 517–528 (1999).
65. Grimm, A. M., Vera, C. S. & Mechoso, C. R. in *The Global Monsoon System: Research and Forecast* (eds Chang, C.-P., Wang, B. & Lau, N.-C. G.) 219–238 (WMO, 2005).
66. Marengo, J. A. et al. Recent developments on the South American monsoon system. *Int. J. Climatol.* **32**, 1–21 (2012).
67. Kodama, Y.-M. Large-scale common features of subtropical precipitation zones (the Baiu frontal zone, the SPCZ, and the SACZ). Part I: characteristics of subtropical frontal zones. *J. Meteorol. Soc. Jpn. Ser. II* **70**, 813–836 (1992).
68. Lenters, J. D. & Cook, K. H. On the origin of the Bolivian high and related circulation features of the South American climate. *J. Atmos. Sci.* **54**, 656–678 (1997).
69. Vera, C. et al. The South American low-level jet experiment. *Bull. Am. Meteorol. Soc.* **87**, 63–78 (2006).
70. Zhou, J. & Lau, K.-M. Does a monsoon climate exist over South America? *J. Clim.* **11**, 1020–1040 (1998).
71. Carvalho, L. M. V., Jones, C. & Liebmann, B. The South Atlantic convergence zone: intensity, form, persistence, and relationships with intraseasonal to interannual activity and extreme rainfall. *J. Clim.* **17**, 88–108 (2004).
72. Marengo, J. A. et al. Climatology of the low-level jet east of the Andes as derived from the NCEP–NCAR reanalyses: characteristics and temporal variability. *J. Clim.* **17**, 2261–2280 (2004).
Illustrates that the South American low-level jet occurs all year long, bringing tropical moist air masses from the Amazon to southern Brazil–northern Argentina more frequently in the warm season, but tropical maritime air more frequently during the cold season.
73. Liebmann, B. et al. Subseasonal variations of rainfall in South America in the vicinity of the low-level jet east of the Andes and comparison to those in the South Atlantic convergence zone. *J. Clim.* **17**, 3829–3842 (2004).
74. Salio, P., Nicolini, M. & Zipser, E. J. Mesoscale convective systems over southeastern South America and their relationship with the South American low-level jet. *Mon. Weather Rev.* **135**, 1290–1309 (2007).
75. Fuenzalida, H., Sánchez, R. & Garreaud, R. D. A climatology of cutoff lows in the Southern Hemisphere. *J. Geophys. Res. Atmos.* **110**, D18101 (2005).
76. Viale, M., Valenzuela, R., Garreaud, R. D. & Ralph, R. M. Impacts of atmospheric rivers on precipitation in southern South America. *J. Hydrometeorol.* **19**, 1671–1687 (2018).
77. Gimeno, L. et al. Major mechanisms of atmospheric moisture transport and their role in extreme precipitation events. *Annu. Rev. Environ. Resour.* **41**, 117–141 (2016).
78. Hu, Z. Z., Huang, B., Zhu, J., Kumar, A. & McPhaden, M. J. On the variety of coastal El Niño events. *Clim. Dyn.* **52**, 7537–7552 (2019).
79. Takahashi, K. & Dewitte, B. Strong and moderate nonlinear El Niño regimes. *Clim. Dyn.* **46**, 1627–1645 (2016).
80. Chiang, J. C. H., Kushnir, Y. & Giannini, A. Deconstructing Atlantic intertropical convergence zone variability: influence of the local cross-equatorial sea surface temperature gradient and remote forcing from the eastern equatorial Pacific. *J. Geophys. Res. Atmos.* **107**, ACL 3-1–ACL 3-19 (2002).
81. Grimm, A. M. The El Niño impact on the summer monsoon in Brazil: regional processes versus remote influences. *J. Clim.* **16**, 263–280 (2003).
82. Grimm, A. M. & Ambrizzi, T. in *Past Climate Variability in South America and Surrounding Regions. Developments in Paleoenvironmental Research* Vol. 14 (eds Vimeaux, F., Sylvestre, F. & Khodri, M.) 159–191 (Springer, 2009).
83. Sasaki, W., Doi, T., Richards, K. J. & Masumoto, Y. The influence of ENSO on the equatorial Atlantic precipitation through the Walker circulation in a CGCM. *Clim. Dyn.* **44**, 191–202 (2015).
84. Ropelewski, C. F. & Bell, M. A. Shifts in the statistics of daily rainfall in South America conditional on ENSO phase. *J. Clim.* **21**, 849–865 (2008).
85. Fernández-Álamo, M. A. & Färber-Lorda, J. Zooplankton and the oceanography of the eastern tropical Pacific: a review. *Prog. Oceanogr.* **69**, 318–359 (2006).
86. Wallace, J. M. & Gutzler, D. S. Teleconnections in the geopotential height field during the northern hemisphere winter. *Mon. Weather Rev.* **109**, 784–812 (1981).
87. Horel, J. D. & Wallace, J. M. Planetary-scale atmospheric phenomena associated with the Southern Oscillation. *Mon. Weather Rev.* **109**, 813–829 (1981).
88. Mo, K. C. & Ghil, M. Statistics and dynamics of persistent anomalies. *J. Atmos. Sci.* **44**, 877–902 (1987).
Finds that an equivalent barotropic-wave-train pattern of circulation anomalies — the Pacific–South American (PSA) pattern — occurs in response to anomalous convective heating in the equatorial Pacific, extending over the south Pacific Ocean to South America.
89. Karoly, D. J. Southern hemisphere circulation features associated with El Niño–Southern Oscillation events. *J. Clim.* **2**, 1239–1252 (1989).
90. Mo, K. C. Relationships between low-frequency variability in the southern hemisphere and sea surface temperature anomalies. *J. Clim.* **13**, 3599–3610 (2000).
91. Cazes-Boezio, G., Robertson, A. W. & Mechoso, C. R. Seasonal dependence of ENSO teleconnections over South America and relationships with precipitation in Uruguay. *J. Clim.* **16**, 1159–1176 (2003).
92. Silva, G. A. M. & Ambrizzi, T. Inter-El Niño variability and its impact on the South American low-level jet east of the Andes during austral summer–two case studies. *Adv. Geosci.* **6**, 283–287 (2006).

93. Montini, T. L., Jones, C. & Carvalho, L. M. The South American low-level jet: a new climatology, variability, and changes. *J. Geophys. Res. Atmos.* **124**, 1200–1218 (2019).
94. Diaz, A. F., Studzinski, C. D. & Mechoso, C. R. Relationships between precipitation anomalies in Uruguay and southern Brazil and sea surface temperature in the Pacific and Atlantic oceans. *J. Clim.* **11**, 251–271 (1998).
95. Rutllant, J. & Fuenzalida, H. Synoptic aspects of the central Chile rainfall variability associated with the southern oscillation. *Int. J. Climatol.* **11**, 63–76 (1991).
96. Hastenrath, S. Circulation and teleconnection mechanisms of northeast Brazil droughts. *Prog. Oceanogr.* **70**, 407–415 (2006).
97. Xie, S.-P. & Philander, S. G. H. A coupled ocean–atmosphere model of relevance to the ITCZ in the eastern Pacific. *Tellus A* **46**, 340–350 (1994).
98. Chang, P., Ji, L. & Li, H. A decadal climate variation in the tropical Atlantic Ocean from thermodynamic air–sea interactions. *Nature* **385**, 516–518 (1997).
99. Nobre, P. & Shukla, J. Variations of sea surface temperature, wind stress, and rainfall over the tropical Atlantic and South America. *J. Clim.* **9**, 2464–2479 (1996).
Shows that north-eastern Brazil droughts are a local manifestation of a large-scale rainfall-anomaly pattern encompassing the whole equatorial Atlantic and Amazon region, related to an early withdrawal of the intertropical convergence zone towards the warm SST anomalies over the northern tropical Atlantic.
100. Chiang, J. C. H. & Vimont, D. Analogous Pacific and Atlantic meridional modes of tropical atmosphere–ocean variability. *J. Clim.* **17**, 4143–4158 (2004).
101. Pezzi, L. P. & Cavalcanti, I. F. A. The relative importance of ENSO and tropical Atlantic sea surface temperature anomalies for seasonal precipitation over South America: a numerical study. *Clim. Dyn.* **17**, 205–212 (2001).
102. Kayano, M. T., Andreoli, R. V., de Souza, R. A. F. & Garcia, S. R. Spatiotemporal variability modes of surface air temperature in South America during the 1951–2010 period: ENSO and non-ENSO components. *Int. J. Climatol.* **37**, 1–13 (2017).
103. Li, Y. et al. Two leading modes of the interannual variability in South American surface air temperature during austral winter. *Clim. Dyn.* **51**, 2141–2156 (2018).
104. Capotondi, A. et al. Understanding ENSO diversity. *Bull. Am. Meteorol. Soc.* **96**, 921–938 (2015).
105. Cai, W. et al. ENSO and greenhouse warming. *Nat. Clim. Change* **5**, 849–859 (2015).
106. Cai, W. et al. Increased variability of eastern Pacific El Niño under greenhouse warming. *Nature* **564**, 201–206 (2018).
107. Kug, J. S., Jin, F. F. & An, S.-I. Two types of El Niño events: cold tongue El Niño and warm pool El Niño. *J. Clim.* **22**, 1499–1515 (2009).
108. Mosquera-Vásquez, K., Dewitte, B. & Illig, S. The Central Pacific El Niño intraseasonal Kelvin wave. *J. Geophys. Res. Oceans* **119**, 6605–6621 (2014).
109. Frauen, C., Dommenget, D., Tyrrell, N., Rezny, M. & Wales, S. Analysis of the nonlinearity of El Niño–Southern Oscillation teleconnections. *J. Clim.* **27**, 6225–6244 (2014).
Finds that the atmospheric-circulation response is stronger for El Niño events compared with La Niña, and for eastern Pacific compared with central Pacific ENSO events, leading to strong regional differences in ENSO teleconnections.
110. Lee, T. & McPhaden, M. J. Increasing intensity of El Niño in the central-equatorial Pacific. *Geophys. Res. Lett.* **37**, L14603 (2010).
111. McPhaden, M. J., Lee, T. & McClurg, D. El Niño and its relationship to changing background conditions in the tropical Pacific Ocean. *Geophys. Res. Lett.* **38**, L15709 (2011).
112. Yeh, S. W., Kirtman, B. P., Kug, J. S., Park, W. & Latif, M. Natural variability of the central Pacific El Niño event on multi-centennial timescales. *Geophys. Res. Lett.* **38**, L02704 (2011).
Shows that variations in the frequency of central Pacific El Niño versus that of eastern Pacific El Niño can occur without forcing of greenhouse warming.
113. Hill, K. J., Taschetto, A. S. & England, M. H. Sensitivity of South American summer rainfall to tropical Pacific Ocean SST anomalies. *Geophys. Res. Lett.* **38**, L01701 (2011).
Shows opposite rainfall responses when SST warming occurs in the eastern as opposed to the western half of the equatorial Pacific.
114. Lavado-Casimiro, W. & Espinoza, J. C. Impacts of El Niño and La Niña in the precipitation over Perú (1965–2007). *Rev. Bras. Meteorol.* **29**, 171–182 (2014).
115. Vicente-Serrano, S. M. et al. The complex influence of ENSO on droughts in Ecuador. *Clim. Dyn.* **48**, 405–427 (2017).
116. Rodrigues, R. R., Campos, E. J. D. & Haarsma, R. The impact of ENSO on the South Atlantic subtropical dipole mode. *J. Clim.* **28**, 2691–2705 (2015).
117. Amaya, D. J. & Foltz, G. R. Impacts of canonical and Modoki El Niño on tropical Atlantic SST. *J. Geophys. Res. Oceans* **119**, 777–789 (2014).
118. Taschetto, A. S., Rodrigues, R. R., Meehl, G. A., McGregor, S. & England, M. H. How sensitive are the Pacific–tropical North Atlantic teleconnections to the position and intensity of El Niño-related warming? *Clim. Dyn.* **46**, 1841–1860 (2016).
119. Navarro-Monterroza, E., Arias, P. A. & Vieira, S. C. El Niño-Oscilación del Sur, fase Modoki, y sus efectos en la variabilidad espacio-temporal de la precipitación en Colombia. *Rev. Acad. Colomb. Cienc. Exactas Fis. Nat.* **43**, 120–132 (2019).
120. Grimm, A. M., Pal, J. S. & Giorgi, F. Connection between spring conditions and peak summer monsoon rainfall in South America: role of soil moisture, surface temperature, and topography in eastern Brazil. *J. Clim.* **20**, 5929–5945 (2007).
121. Barreiro, M. & Díaz, N. Land–atmosphere coupling in El Niño influence over South America. *Atmos. Sci. Lett.* **12**, 351–355 (2011).
122. Builes-Jaramillo, A., Marwan, N., Poveda, G. & Kurths, J. Nonlinear interactions between the Amazon River basin and the Tropical North Atlantic at interannual timescales. *Clim. Dyn.* **50**, 2951–2969 (2018).
Shows that a lower-than-normal rainfall over the Amazon basin decreases the pressure gradient between the Amazon and the tropical North Atlantic, weakens the north-easterly trades, intensifies warming of the tropical North Atlantic, in turn, reinforcing the rainfall decrease over the Amazon basin.
123. Dewitte, B. & Takahashi, K. Diversity of moderate El Niño events evolution: role of air–sea interactions in the eastern tropical Pacific. *Clim. Dyn.* **52**, 7455–7476 (2019).
124. Haarsma, R. J., Campos, E. J. D. & Molteni, F. Atmospheric response to South Atlantic SST dipole. *Geophys. Res. Lett.* **30**, 1864 (2003).
125. Jahfer, S., Vinayachandran, P. N. & Nanjundiah, R. S. Long-term impact of Amazon river runoff on northern hemispheric climate. *Sci. Rep.* **7**, 10989 (2017).
126. Poveda, G., Gil, M. M. & Quiceno, N. The annual cycle of Colombia's hydrology and its relationship with ENSO and NAO. *Bull. Am. Meteorol. Soc.* **27**, 721–731 (1998).
127. Taschetto, A. S. & Ambrizzi, T. Can Indian Ocean SST anomalies influence South American rainfall? *Clim. Dyn.* **38**, 1615–1628 (2012).
128. Chan, S. C., Behera, S. K. & Yamagata, T. Indian Ocean Dipole influence on South American rainfall. *Geophys. Res. Lett.* **35**, L14S12 (2008).
Outlines that a positive Indian Ocean Dipole excites a dipolar pattern in rainfall anomalies, with reduced rainfall over central Brazil but increased rainfall over La Plata Basin during austral spring.
129. Cai, W., van Rensch, P., Cowan, T. & Hendon, H. H. Teleconnection pathways of ENSO and the IOD and the mechanisms for impacts on Australian rainfall. *J. Clim.* **24**, 3910–3923 (2011).
130. Vera, C. S. & Osman, M. Activity of the Southern Annular Mode during 2015–2016 El Niño event and its impact on Southern Hemisphere climate anomalies. *Int. J. Climatol.* **38**, e1288–e1295 (2018).
131. Leõn-Muñoz, J. et al. Hydroclimatic conditions trigger record harmful algal bloom in western Patagonia (summer 2016). *Sci. Rep.* **8**, 1330 (2018).
132. An, S. I. & Wang, B. Interdecadal change of the structure of the ENSO mode and its impact on the ENSO frequency. *J. Clim.* **13**, 2044–2055 (2000).
133. da Silva, G. A. M., Drumond, A. & Ambrizzi, T. The impact of El Niño on South American summer climate during different phases of the Pacific decadal oscillation. *Theor. Appl. Climatol.* **106**, 307–319 (2011).
134. Poveda, G., Alvarez, D. M. & Rueda, O. A. Hydroclimatic variability over the Andes of Colombia associated with ENSO: a review of climatic processes and their impact on one of the Earth's most important biodiversity hotspots. *Clim. Dyn.* **36**, 2233–2249 (2011).
135. Wang, G. & Cai, W. Climate-change impact on the 20th-century relationship between the Southern Annular Mode and global mean temperature. *Sci. Rep.* **3**, 2039 (2013).
136. Ham, Y. G., Choi, J. Y. & Kug, J. S. The weakening of the ENSO–Indian Ocean Dipole (IOD) coupling strength in recent decades. *Clim. Dyn.* **49**, 249–261 (2017).
137. McGregor, S. et al. Recent Walker circulation strengthening and Pacific cooling amplified by Atlantic warming. *Nat. Clim. Change* **4**, 888–892 (2014).
138. Wang, L., Yu, J.-Y. & Paek, H. Enhanced biennial variability in the Pacific due to Atlantic capacitor effect. *Nat. Commun.* **8**, 14887 (2017).
Shows that a warmer Atlantic since the early 1990s — a result of the positive phase of Atlantic multidecadal oscillation and a global warming trend — has enhanced the biennial cycle of ENSO events.
139. Cai, W. & Cowan, T. Trends in Southern Hemisphere circulation in IPCC AR4 models over 1950–99: Ozone depletion versus greenhouse forcing. *J. Clim.* **20**, 681–693 (2007).
140. Barnston, A. G. et al. Verification of the first 11 years of IRI's seasonal climate forecasts. *J. Appl. Meteorol. Climatol.* **49**, 493–520 (2010).
141. Bombardi, R. J. et al. Seasonal predictability of summer rainfall over South America. *J. Clim.* **31**, 8181–8195 (2018).
142. Zhao, M., Hendon, H. H., Alves, O., Liu, G. & Wang, G. Weakened Eastern Pacific El Niño predictability in the early twenty-first century. *J. Clim.* **29**, 6805–6822 (2016).
143. Giannini, A., Chiang, J. C. H., Cane, M. A., Kushnir, Y. & Seager, R. The ENSO teleconnection to the tropical Atlantic Ocean: contributions of the remote and local SSTs to rainfall variability in the tropical Americas. *J. Clim.* **14**, 4530–4544 (2001).
144. Richter, I. et al. On the triggering of Benguela Niños: remote equatorial versus local influences. *Geophys. Res. Lett.* **37**, L20604 (2010).
145. Barreiro, M. Influence of ENSO and the South Atlantic Ocean on climate predictability over southeastern South America. *Clim. Dyn.* **35**, 1493–1508 (2010).
146. Keenlyside, N. S., Ding, H. & Latif, M. Potential of equatorial Atlantic variability to enhance El Niño prediction. *Geophys. Res. Lett.* **40**, 2278–2283 (2013).
147. Luo, J.-J., Liu, G., Hendon, H., Alves, O. & Yamagata, T. Inter-basin sources for two-year predictability of the multi-year La Niña event in 2010–2012. *Sci. Rep.* **7**, 2276 (2017).
148. Ren, H. L., Zuo, J. & Deng, Y. Statistical predictability of Niño indices for two types of ENSO. *Clim. Dyn.* **52**, 5361–5382 (2019).
149. Dayan, H., Vialard, J., Izumo, T. & Lengaigne, M. Does sea surface temperature outside the tropical Pacific contribute to enhanced ENSO predictability? *Clim. Dyn.* **43**, 1311–1325 (2014).
150. Chikamoto, Y. et al. Skilful multi-year predictions of tropical trans-basin climate variability. *Nat. Commun.* **6**, 6869 (2015).
151. Boulanger, J.-P., Martinez, F. & Segura, E. C. Projection of future climate change conditions using IPCC simulations, neural networks and Bayesian statistics. Part 2: precipitation mean state and seasonal cycle in South America. *Clim. Dyn.* **28**, 255–271 (2007).
152. Junquas, C., Vera, C. S., Li, L. & Le Treut, H. Impact of projected SST changes on summer rainfall in southeastern South America. *Clim. Dyn.* **40**, 1569–1589 (2013).
153. Jones, C. & Carvalho, L. M. V. Climate change in the South American monsoon system: present climate and CMIP5 projections. *J. Clim.* **26**, 6660–6678 (2013).
154. Li, W., Fu, R. & Dickinson, R. E. Rainfall and its seasonality over the Amazon in the 21st century as assessed by the coupled models for the IPCC AR4. *J. Geophys. Res. Atmos.* **111**, D02111 (2006).
Shows that an El Niño-like sea-surface temperature change and warming in the northern tropical Atlantic enhances atmospheric subsidence and reduces clouds over the Amazon.
155. Bombardi, R. & Carvalho, L. IPCC global coupled model simulations of the South America monsoon system. *Clim. Dyn.* **33**, 893–916 (2009).
156. Karamperidou, C., Jin, F. F. & Conroy, J. L. The importance of ENSO nonlinearities in tropical Pacific response to external forcing. *Clim. Dyn.* **49**, 2695–2704 (2017).
157. Grimm, A. M. & Natori, A. A. Climate change and interannual variability of precipitation in South America. *Geophys. Res. Lett.* **33**, L19706 (2006).

158. da Rocha, R. P., Reboita, M. S., Dutra, L. M. M., Llopart, M. P. & Coppola, E. Interannual variability associated with ENSO: present and future climate projections of RegCM4 for South America-CORDEX domain. *Clim. Change* **125**, 95–109 (2014).
159. Perry, S. J., McGregor, S., Gupta, A. S., England, M. H. & Maher, N. Projected late 21st century changes to the regional impacts of the El Niño-Southern Oscillation. *Clim. Dyn.* **54**, 395–412 (2020).
160. Cai, W. et al. Increased frequency of extreme La Niña events under greenhouse warming. *Nat. Clim. Change* **5**, 132–137 (2015).
161. Christidis, N., Betts, R. A. & Stott, P. A. The extremely wet March of 2017 in Peru. *Bull. Am. Meteorol. Soc.* **100**, S31–S35 (2019).
162. Kim, J. S., Kug, J. S. & Jeong, S. J. Intensification of terrestrial carbon cycle related to El Niño–Southern oscillation under greenhouse warming. *Nat. Commun.* **8**, 1674 (2017).
163. Power, S. B. & Delage, F. P. D. El Niño–Southern Oscillation and associated climatic conditions around the world during the latter half of the twenty-first century. *J. Clim.* **31**, 6189–6207 (2018).
164. Blázquez, J. & Nuñez, M. N. Analysis of uncertainties in future climate projections for South America: comparison of WCRP-CMIP3 and WCRP-CMIP5 models. *Clim. Dyn.* **41**, 1039–1056 (2013).
165. Tedeschi, R. G. & Collins, M. The influence of ENSO on South American precipitation: simulation and projection in CMIP5 models. *Int. J. Climatol.* **37**, 3319–3339 (2017).
166. Mora, C. et al. Global risk of deadly heat. *Nat. Clim. Change* **7**, 501–506 (2017).
167. Zilli, M. T., Carvalho, L. M. V. & Lintner, B. R. The poleward shift of South Atlantic Convergence Zone in recent decades. *Clim. Dyn.* **52**, 2545–2563 (2019).
168. Bedoya-Soto, J. M., Poveda, G., Trenberth, K. E. & Vélez-Upegui, J. J. Interannual hydroclimatic variability and the 2009–2011 extreme ENSO phases in Colombia: from Andean glaciers to Caribbean lowlands. *Theor. Appl. Climatol.* **135**, 1531–1544 (2019).
169. Moy, C., Seltzer, G., Rodbell, D. & Anderson, D. Variability of El Niño/Southern Oscillation activity at millennial timescales during the Holocene epoch. *Nature* **420**, 162–165 (2002).
170. Rodbell, D. et al. An ~15,000-year record of El Niño-driven alluviation in southwestern Ecuador. *Science* **283**, 516–520 (1999).
Uses inorganic laminae in an alpine lake near Ecuador to show that El Niño periodicity increases from ~15 years 15,000–7,000 years before present to 2–8.5 years in the modern climate.
171. Conroy, J., Overpeck, J., Cole, J., Shanahan, T. & Steinitz-Kannan, M. Holocene changes in eastern tropical Pacific climate inferred from a Galápagos lake sediment record. *Quat. Sci. Rev.* **27**, 1166–1180 (2008).
172. Clement, A. C., Seager, R. & Cane, M. A. Orbital controls on the El Niño/Southern Oscillation and the tropical climate. *Paleoceanography* **14**, 441–456 (1999).
173. Karamperidou, C., Di Nezio, P. N., Timmermann, A., Jin, F. F. & Cobb, K. M. The response of ENSO flavors to mid-Holocene climate: implications for proxy interpretation. *Paleoceanography* **30**, 527–547 (2015).
174. Li, G. & Xie, S.-P. Tropical biases in CMIP5 multimodel ensemble: the excessive equatorial Pacific cold tongue and double ITCZ problems. *J. Clim.* **27**, 1765–1780 (2014).
175. Bellucci, A., Gualdi, S. & Navarra, A. The double-ITCZ syndrome in coupled general circulation models: the role of large-scale vertical circulation regimes. *J. Clim.* **23**, 1127–1145 (2010).
176. Cai, W. & Cowan, T. Why is the amplitude of the Indian Ocean Dipole overly large in CMIP3 and CMIP5 climate models? *Geophys. Res. Lett.* **40**, 1200–1205 (2013).
177. McGregor, S., Stuecker, M. F., Kajtar, J. B., England, M. H. & Collins, M. Model tropical Atlantic biases underpin diminished Pacific decadal variability. *Nat. Clim. Change* **8**, 493–498 (2018).
178. Cai, W., Hendon, H. H. & Meyers, G. A. Indian Ocean dipolelike variability in the CSIRO Mark 3 coupled climate model. *J. Clim.* **18**, 1449–1468 (2005).
179. Taschetto, A. S. et al. Cold tongue and warm pool ENSO events in CMIP5: mean state and future projections. *J. Clim.* **27**, 2861–2885 (2014).
180. Ma, H. Y. et al. Impact of land surface processes on the South American warm season climate. *Clim. Dyn.* **37**, 187–203 (2011).
181. Yin, L., Fu, R., Shevliakova, E. & Dickinson, R. E. How well can CMIP5 simulate precipitation and its controlling processes over tropical South America? *Clim. Dyn.* **41**, 3127–3143 (2013).
182. Misra, V., Dirmeyer, P. A. & Kirtman, B. P. Dynamic downscaling of seasonal simulations over South America. *J. Clim.* **16**, 103–117 (2003).
183. Solman, S. A., Nunez, M. N. & Cabré, M. F. Regional climate change experiments over southern South America. I: present climate. *Clim. Dyn.* **30**, 533–552 (2008).
184. Cavalcanti, I. F., Goddard, L. & Kirtman, B. The future of seasonal prediction in the Americas. *VAMOS Newsl.* **3**, 3–7 (2006).
185. Grimm, A. M. in *Tropical Extremes: Natural Variability and Trends* (eds Vuruputur, V., Sukhatme, J., Murtugudde, R. & Roca, R.) 51–93 (Elsevier, 2018).
186. Rodrigues, R. R., Taschetto, A. S., Gupta, A. S. & Foltz, G. R. Common cause for severe droughts in South America and marine heatwaves in the South Atlantic. *Nat. Geosci.* **12**, 620–626 (2019).
Finds that drought in eastern South America and marine heatwaves in the adjacent south Atlantic Ocean are concurrently triggered by tropical convection in the Indian and Pacific oceans, which causes Rossby wave trains with a persistent anticyclonic circulation over the region.
187. Erfanian, A., Wang, G. & Fomenko, L. Unprecedented drought over tropical South America in 2016: significantly under-predicted by tropical SST. *Sci. Rep.* **7**, 5811 (2017).
188. Foley, J. A., Botta, A., Coe, M. T. & Costa, M. H. El Niño–Southern oscillation and the climate, ecosystems and rivers of Amazonia. *Glob. Biogeochem. Cycles* **16**, 79-1–79-20 (2002).
189. Withey, K. et al. Quantifying immediate carbon emissions from El Niño-mediated wildfires in humid tropical forests. *Philos. Trans. R. Soc. Lond. B Biol. Sci.* **373**, 20170312 (2018).
190. Schneider, U., Fuchs, T., Meyer-Christoffer, A. & Rudolf, B. Global precipitation analysis products of the GPCC. *dwd.de* https://www.dwd.de/EN/ourservices/gpcc/gpcc.html (2008).
191. Kalnay, E. et al. The NCEP/NCAR 40-year reanalysis project. *Bull. Am. Meteorol. Soc.* **77**, 437–472 (1996).
192. Rayner, N. A. et al. Global analyses of sea surface temperature, sea ice, and night marine air temperature since the late nineteenth century. *J. Geophys. Res. Atmos.* **108**, 4407 (2003).
193. Taylor, K. E., Stouffer, R. J. & Meehl, G. A. An overview of CMIP5 and the experimental design. *Bull. Am. Meteorol. Soc.* **93**, 485–498 (2012).

Acknowledgements
This work is supported by the National Key R&D Program of China (2018YFA0605700). W.C., A.S., B.N. and G.W. are supported by the CSHOR and the Earth System and Climate Change Hub of the Australian Government's National Environment Science Program. The CSHOR is a joint research Centre for Southern Hemisphere Oceans Research between the Qingdao National Laboratory for Marine Science and Technology (QNLM) and the Commonwealth Scientific and Industrial Research Organisation (CSIRO). R.R. is supported by CNPq grant (401873/2016-1), CAPES (88881.145866/2017-1), Program INCT-MCII and Rede CLIMA. A.M.G. acknowledges the support of CNPq (Brazil). A.S.T. is supported by the Australian Research Council (ARC FT160100495). B.D. is supported by Fondecyt grant (1171861) and ANR. G.P. is supported by Universidad Nacional de Colombia at Medellin, Colombia. Y.-G.H. is funded by the Korea Meteorological Administration Research and Development Program under grant (KMI2018-07010). W.A. is supported from the Earth Institute Postdoctoral Fellows program. J.M. is supported by the National Institute of Science and Technology for Climate Change Phase 2 under CNPq grant (465501/2014-1), FAPESP grant (2014/50848-9) and CAPES grant (88887.136402-00INCT). L.M.A. is supported by Sao Paulo Research Foundation Grant FAPESP (#2015/50122-0), DFG-GRTK (1740/2) and INCR-Climate change project Phase 2 (CNPq465501/2014-1/Public call MCTI/CNPQ/CAPES/FAPS no. 16/2014). L.W. is supported by the National Natural Science Foundation of China projects (41490640 and 41490643). C.K. is supported by US NSF award (AGS-1902970). M.J.M. is supported by NOAA. This is PMEL contribution no. 5039. M.O. and C.V were supported by Consejo Nacional de Investigaciones Científicas y Técnicas (CONICET) PIP 112-20120100626CO, UBACyT 20020130100489BA and Belmont Forum/ANR-15-JCL/-0002-01 CLIMAX.

Author contributions
W.C. and M.J.M. conceived the study. M.J.M., A.M.G., R.R., A.S.T., B.D. and A.S. coordinated the presentation and discussion for various sections. All authors contributed to the manuscript preparation, interpretation, discussion and writing, led by W.C.

Competing interests
The authors declare no competing interests.

Peer Review information
Nature Reviews Earth & Environment thanks C. Frauen, R. Tedeschi and the other, anonymous, reviewer(s), for their contribution to the peer review of this work.

Publisher's note
Springer Nature remains neutral with regard to jurisdictional claims in published maps and institutional affiliations.